Petroleum Science 18 (2021) 1370–1389

Contents lists available at ScienceDirect

Petroleum Science

journal homepage: www.keaipublishing.com/en/journals/petroleum-science

Original Paper

Study on brittleness templates for shale gas reservoirs-A case study of Longmaxi shale in Sichuan Basin, southern China

Qamar Yasin [a, b], Ghulam Mohyuddin Sohail [c, d], Ke-Yu Liu [a], Qi-Zhen Du [a, b, *], Cyril D. Boateng [a]

[a] The Key Laboratory of Deep Oil and Gas, China University of Petroleum (East China), Qingdao, 266580, China
[b] Qingdao National Laboratory for Marine Science and Technology, Laboratory for Marine Mineral Resources, Qingdao, 266237, China
[c] Department of Civil, Geological and Environmental Engineering, University of Saskatchewan, Saskatoon, S7N 5C5, Canada
[d] Department of Geological Engineering, University of Engineering and Technology, Lahore, Pakistan

ARTICLE INFO

Article history:
Received 29 August 2020
Accepted 24 May 2021
Available online 21 September 2021

Edited by Jie Hao

Keywords:
Brittleness index
Geomechanical properties
Petrophysical parameters
Longmaxi shale

ABSTRACT

Differentiating brittle zones from ductile zones in low permeability shale formations is imperative for efficient hydraulic fracturing stimulation. The brittleness index (BI) is used to describe the rock resistance to hydraulic fracture initiation and propagation and measures the ease at which complex fracture networks can be created. In this study, we constructed brittleness templates through the correlation of fundamental rock properties and geomechanical characterization. We then employed the templates to distinguish the brittle, ductile, and brittle-ductile transition zones in the Longmaxi shale gas reservoir, Sichuan Basin of southern China. The approach works in two steps. First, we suggest a new expression for the mineralogical BI by their respective weights based on the analysis of correlation coefficients between mechanical testing and XRD results. Second, we correlate TOC, porosity, pore fluid, natural fractures, and improved BI model with multiple elastic properties to define the brittle, ductile, and transitional zones in the Longmaxi shale gas reservoir of China. Compared with the traditional mineralogy-based BI definition, the improved BI model differentiates the brittle and ductile zones and provides a better sense of the most suitable fracturing regions. Our results show that the brittleness templates, which combine fundamental rock properties, improved BI model, and geomechanical characterization led to identifying favorable zones for hydraulic fracturing and enhanced shale characterization. The proposed brittleness templates' effectiveness was verified using data from horizontal wells, offset wells, shale gas wells from different origins, laboratory core testing, and seismic inversion of BI across the studied wells.

1. Introduction

The Silurian Longmaxi shale distributed in the southern Sichuan Basin exhibits overall ultra-low matrix permeability. Generally, shale with ultra-low permeability requires efficient multi-stage hydraulic fracturing (informally referred to as fracking) technology to enhance initial gas production (Li et al., 2018). A complex fracture network is generated during multi-stage fracking and connected with pre-existing natural fractures to produce gas and ultimately enhances production (Yasin et al., 2017). The effectiveness of hydraulic fracturing is strongly dependent on mechanical rock properties (Sohail et al., 2020). In this context, scientists often use the term brittleness, a critical rock mechanical property used to describe the rock's ability to hydraulically fracture (Shia et al., 2016; Kim et al., 2017). The brittleness plays a significant role in identifying the possible failure features under hydraulic fracturing in shale gas. It is primarily controlled by the mineralogical composition and has been widely accepted as a critical characteristic of well stimulation's potential effectiveness (Jarvie et al., 2007). The more reliable and direct method to investigate shale brittleness is to develop laboratory testing (Lashkaripour et al., 2018). However, laboratory testing requires core plugs, and core analysis data is limited to zones or specific wells (Yasin et al., 2019).

For hydraulic fracturing treatments in gas-bearing shales, engineers require a continuous profile of brittleness information over a sizeable horizontal span. We can only obtain this information directly from well logs (Li et al., 2018). Though there are several BI

* Corresponding author. The Key Laboratory of Deep Oil and Gas, China University of Petroleum (East China), Qingdao, 266580, China.
E-mail address: multicomponent@163.com (Q.-Z. Du).

https://doi.org/10.1016/j.petsci.2021.09.030

estimating methods in the literature, there is no consensus on a standard prediction tool for brittleness (Ozfirat et al., 2016). Rock behavior is controlled by many factors, including strain rate, temperature, pressure, saturation, TOC, rock mineralogy, and in situ stress making lots of brittleness descriptions and characterizations. A detailed description of the variety of brittleness indices based on the static mechanical properties, rock's composition, and elastic parameters measured from S-wave and P-wave sonic logs or seismic survey has been stated in our previous paper (Yasin et al., 2018a). As an alternative index, Grieser and Bray (2007), Jarvie et al. (2007), Rickman et al. (2008), Wang and Gale (2009), and Jin et al. (2014) proposed the definition of brittleness from a different aspect of rock composition. Table 1 summarizes the models that determine the brittleness based on mineralogical composition. Based on these studies, it is evident that a consensus view on the definition of BI based on mineralogy does not yet exist. For instance, Jarvie et al. (2007) proposed BI using quartz content as a significant control of brittleness. In contrast, Wang and Gale (2009) used dolomite and quartz as controls of rock brittleness. Later, Jin et al. (2014) reported that high calcite and quartz contents (including feldspar and mica) account for a rock's high brittleness. The multitude of different definitions of mineralogy-based BI from these researchers yields an inconsistent picture of brittle behavior and a vague understanding of the concept of brittleness.

Recently, Kang et al. (2020) investigated the relationship between the triaxial test and the content of quartz, feldspar, calcite, and dolomite. According to their studies, the simple aggregate of brittle minerals was not statistically correlated to the mechanical BI and provided unreliable shale brittleness. Taking the bulk modulus of various brittle minerals (quartz, dolomite, and calcite), Kang et al. (2020) developed new mineralogy-based BI, which characterizes the weight of each brittle mineral with varying coefficients of weighting. However, the correlation between the new mineralogy-based BI and the mechanical-based BI was not very strong because heavy brittle minerals like mica and pyrite were not considered.

In addition to mineralogy-based BI, researchers proposed several brittleness indices using mechanical testing on the core samples. Yang et al. (2013) reported that the laboratory-based brittleness indices decrease with increasing confining pressure. However, these brittleness indices globally reflect no verification of the rock behavior under hydraulic fracturing conditions. Also, elastic properties-based BI indicates that high TOC shale is relatively ductile (Yasin et al., 2017). Table 2 summarizes the methods based on physical experiments proposed over the past two decades.

Geoscientists and engineers agree that brittleness is a geomechanical property that facilitates hydraulic fracturing instead of geochemical property. According to Amir et al. (2013), brittleness is a material property with high mechanical strength, and the failure behavior exhibits a low degree of inelasticity. Therefore, it is a reasonable approach to estimate rock's brittleness by the geomechanical properties because BI based on mineralogy alone does not indicate rock strength (Ozfirat et al., 2016).

The present study integrates fundamental rock properties (TOC, porosity, mineralogical composition, pore fluid type, and saturation), natural fractures (Li et al., 2016), and geomechanical characterization to develop mechanical earth models. We construct the brittleness templates for classifying the Longmaxi shale regarding brittle, ductile, and transitional behaviors and reservoir characteristics of shale.

The Longmaxi shale hosts a highly productive shale gas play in the Sichuan Basin and produces shale gas in commercial quantities. Many scholars have published that the Longmaxi shale has a relatively large hydrocarbon accumulation than conventional plays in China (Wu et al., 2016; Zhang et al., 2017). Liu et al. (2012) compared the Longmaxi shale with the Barnett shale and found that the Longmaxi shale can be a good shale gas reservoir as it is buried deeper with a higher degree of thermal maturity, more quartz of biogenic silicon, and high gas content. Despite the enormous resources and potential of shale gas in the Longmaxi Formation, verifiable and accurate prediction of brittle regions, especially in organic-rich zones, is challenging because even sophisticated methods proposed in the literature fail to perform effectively (Zhang et al., 2017). This paper aims to developing an improved BI evaluation model based on the depositional environment and specific conditions of the Longmaxi shale rather than repeating the old models proposed for North American shales (Liu et al., 2012). This study also correlates fundamental rock properties, natural fractures, and improved BI models with multiple elastic properties and establishes templates for brittleness evaluation for the Longmaxi shale gas reservoir in the Sichuan Basin, China. According to the results, a strong correlation exists between mineralogical compositions, TOC, geomechanical properties, pre-existing fractures, and improved BI model. The proposed brittleness templates are tested using data from a horizontal well (J-2), an offset vertical well (J-3), and a shale gas well (106) from different locations of the study area with varying shale compositions, laboratory testing (uniaxial compressive test) of several outcrop samples, and a seismic inversion profile of BI across the studied wells.

2. Geological setting and stratigraphy

The Sichuan Basin is a major petroliferous and large sedimentary intracratonic basin, covering about 180,000 km^2. It is located in the western part of the Yangtze Craton (Yangtze Platform), southwestern China (Liang et al., 2012; Zhang et al., 2017). The Sichuan Basin lies along the eastern margin of the Tibetan Plateau and is

Table 1
Method to define rock brittleness based on mineralogical compositions.

Equation	Remark	Reference
$BI = \frac{W_{quartz} + W_{calcite} + W_{dolomite}}{W_{quartz} + W_{carbonate} + W_{clay}} \times 100,$	where W is the weight percentage of essential minerals	Jin et al. (2014)
$BI = \frac{V_{quartz} \times \left(\frac{E_{quartz}}{\upsilon_{quartz}}\right)}{V_{quartz} \times \left(\frac{E_{quartz}}{\upsilon_{quartz}}\right) + V_{calcite} \times \left(\frac{E_{calcite}}{\upsilon_{calcite}}\right) + V_{clay} \times \left(\frac{E_{clay}}{\upsilon_{clay}}\right)} \times 100,$	where E and υ denote Young's modulus and Poisson's ratio of essential minerals.	Diao (2013)
$BI = \frac{[1 + a(R_c - b)] \times C_{quartz}}{C_{quartz} + C_{carbonate} + C_{clay}} \times 100,$	where R_c is morphology maturation rate	Wang (2008)
$BI = \frac{E}{\upsilon},$		Guo (2013)
$BI = \frac{\lambda}{(\lambda + 2\mu_\lambda)},$	where λ is lame constant	Goodway (2010)

Table 2
Methods to determine rock brittleness based on physical experiments.

Equation	Remark	Reference
$BI = \frac{(\sigma_c \times \sigma_t)}{2}$,	where $\sigma_c$is uniaxial compression strength	Altindag (2003)
$BI = \frac{\sqrt{(\sigma_c \times \sigma_t)}}{2}$,	where σ_t is tensile strength	Altindag (2003)
$BI = \frac{(\sigma_p - \sigma_r)}{\sigma_p} \times \frac{\lg\lvert k_{ac}\rvert}{10}$,	where σ_p and σ_r are peak and residual strength, k_{ac} is the stress slope of post-peak	Zhou (2014)
$BI = 1 - \exp\left(\frac{M}{E}\right)$,	where E is Young's modulus	Fjaer et al. (2008)
$BI = \frac{(M - E)}{M}$,	M is the post-peak modulus	Weicht, 2015
$BI = \frac{E}{M}$,		Weicht 2015

bounded by many individual fault zones and fold belts. To the west, the basin is bounded by Longmenshan fault and fold belt (Longmen Mountains), Micang-Daba mountains (Dabashan fold belt) to the north, Daliang-Dalou mountains to the south, and Qiyao mountains (Qiyueshan fold belt) to the east (Fig. 1a). In the passive continental margin, the emergence started from a Sinian-Middle Triassic (Z1-T2), resulted in the deposition of thick sections of interbedded carbonates, clastics, and evaporites of marine sediments with volcanic layers (Fig. 1b). During the Late Triassic, the oceanic subduction of the Yangtze platform and termination of the Palaeotethys has resulted in the deformation of the Sichuan Basin (Huang et al., 2012; Liang et al., 2016). Primarily, the Sichuan Basin was under a foreland basin evolutionary stage, and stresses from this cause uplift, folding, reverse and thrust faults, and erosion. The Sichuan

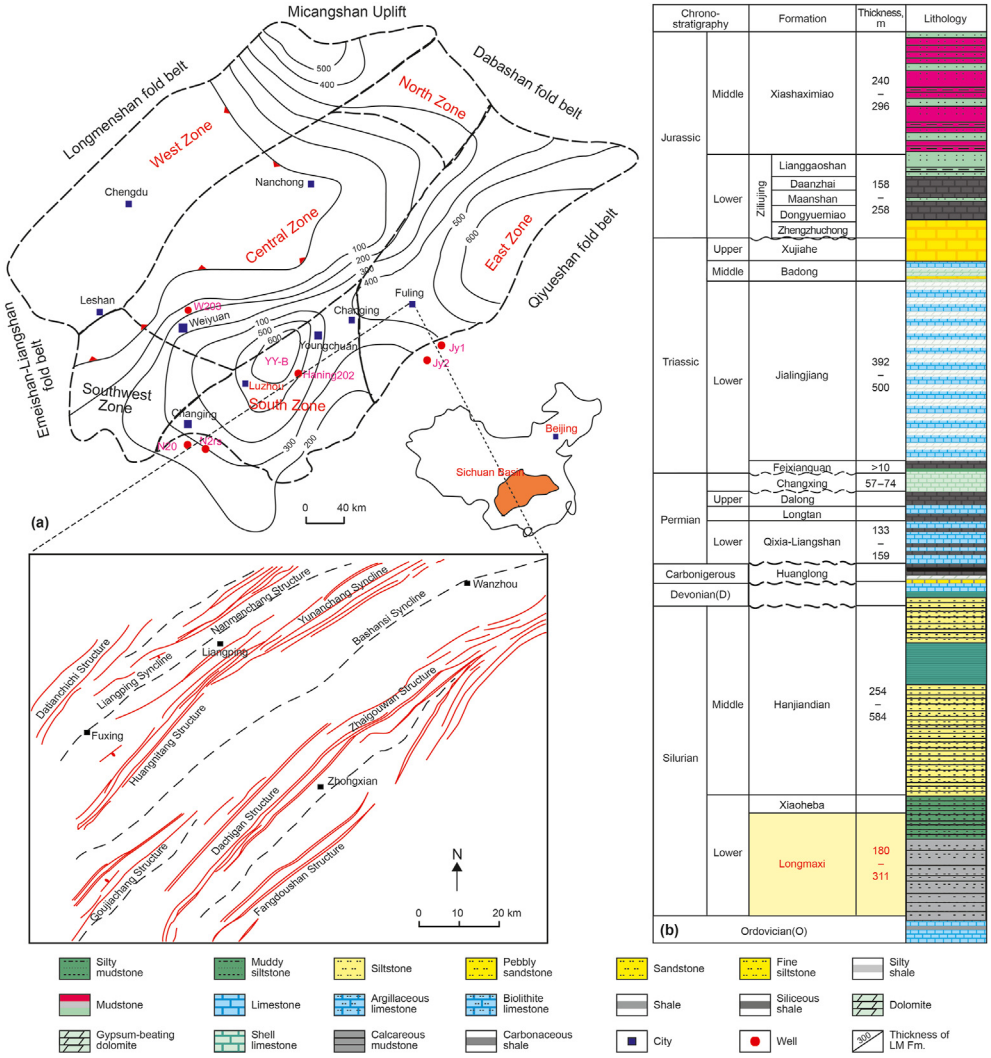

Fig. 1. (a) Isopach of the Longmaxi shale and location of shale gas field in the Sichuan Basin China (modified after Dai et al. (2014)); (b) generalized stratigraphic column showing the lower Silurian Longmaxi shale.

Basin and the periphery have undergone frequent tectonic movement, causing the uplift and forming a series of NE-SW echelon folds (Huang et al., 2012; Liang et al. 2012, 2016). During the Late Ordovician, a confined sea was formed due to the various uplifts which supplied low-energy, deep-water anoxic conditions. The Late Ordovician that continued into the Early Silurian developed the tectonostratigraphic framework with the uplift towards east and west. Due to this extensive tectonic uplift, a group of fine-grained clastic and black shale sedimentary rocks consisting of silt- and clay-sized particles were deposited. At the end of the Silurian period, the sedimentation ceased and led to an erosional unconformity (Huang et al., 2012; Liang et al., 2016).

In the Sichuan Basin, a thick sedimentary fill from Proterozoic (Sinian) to Quaternary strata is developed (Fig. 1b). It is filled with up to 10 km of Late Proterozoic to Quaternary sedimentary deposits. The Lower Silurian Longmaxi Formation was deposited in the Silurian system's shallow-marine environments (Li et al., 2016). It has two sedimentary cycles containing a set of black shale, subordinate gray to dark gray carbonate rocks, gray-black (silty) mudstone, and gray to dark-gray siltstone. In South China, the black shale units of the Longmaxi Formation have a similar sedimentary environment and organic matter enrichment with the basal Silurian 'hot shales' in North Africa and the Middle East. Previous researchers have reported that both the shales were deposited by flooding during the Silurian system (Liang et al., 2012; Dai et al., 2014). The Formation contains good-quality thick shale strata with high TOC and brittle minerals. At the bottom of the Longmaxi Formation, relatively thick pyrites reached their maximum in the Sichuan Basin's southern part. The anoxic environment provided suitable conditions for preserving organic matter to black shale in the Wufeng-Longmaxi Formation. The organic-rich Wufeng-Longmaxi Formation mainly contains the equivalent sapropelic type (types I and II) and mixed oil and gas-prone organic matter (Dai et al., 2014).

The widely distributed Wufeng-Longmaxi shale in the Sichuan Basin has the most significant thickness in eastern Chongqing and western Hubei, with a maximum thickness of over 1000 m. The high TOC Longmaxi shale is also a proven source rock in the Sichuan Basin and surrounding areas (Liang et al. 2016). Several authors have reported the source rock potential of the Longmaxi shale and its importance as an unconventional shale gas play (Li et al., 2016; Jiang et al. 2020). Also, they have noted its characteristics as a source, reservoir, and seal.

3. Materials and methods

3.1. Data description

Borehole logging data from three vertical wells and one horizontal well: J-2, J-3, 106, and J-2H were employed to calculate the petrophysical parameters in Wufeng-Longmaxi shale gas reservoirs. Measured petrophysical parameters (e.g., mineralogical composition, porosity, permeability, density, and total organic carbon content) in Well J-2 were also available for comparison. Besides, ten outcrop samples in the Wufeng-Longmaxi shale were collected from the Sichuan Basin to measure their petrophysical (TOC content and mineralogical composition), UCS (uniaxial compressive strength), and elastic parameters; dynamic and static Young's modulus, dynamic and static Poisson's ratio, bulk and shear moduli. From these samples, we delivered ten cores (5 vertical and 5 horizontal) of standard size (25.4 mm diameter and 50 mm length) to the laboratory for ultrasonic velocity and uniaxial compressive strength (UCS) testing.

We grounded a few samples to evaluate their mineral composition and conduct the XRD analysis with an X'pert PRO MRD system. We measured the TOC content of the same cores by a LECO CS230 carbon/sulfur analyzer. Out of the ten samples, we selected two with horizontal and vertical bedding laminations for identifying micro-features and layering, as shown in Fig. 2a and b. We then used FESEM (Field-emission Scanning Electron Microscope) to take images on selected core samples for identifying organic pore quantity in Wufeng-Longmaxi Formation. The FESEM images indicate that organic pores of nano to micrometer size have good connectivity, as shown in Fig. 2c and d.

3.2. Petrophysical analysis

The gamma-ray (GR), shallow resistivity (RS), deep resistivity (RT), bulk density (DEN), neutron porosity (CNL), shear and compressional sonic (DTP and DTS), photoelectric effect (PEF), and FMI (formation micro-imager) logs were used for estimating mineralogical composition, porosity, total organic carbon (TOC) content and total gas content. The natural fractures were also identified using multiple logs in three vertical and one horizontal wells.

Also, we used the petrophysical parameters measured on core samples of Longmaxi shale from Well J-2. We used the results from the core to calibrate the Elan-based mineralogy (software module for minerals volume estimation using logs and conversion from volume to weight percentage) and log-based TOC.

The mineralogical compositions of the Longmaxi shale samples were determined using a combination of DEN, CNL, RT, GR, PEF, DTP, and DTS logs. The dominant minerals are presumed to have quartz, clay, calcite, dolomite, and pyrite. The identification of such minerals was confirmed by XRD analysis. We omitted minor minerals, such as TOC, from this analysis because they are known to impact log-based mineralogy algorithms. We run more iterations of the Mineral Solver Package (Elan) to minimize errors by varying the following parameters within prescribed limits: mineral endpoints (specific log reading for pure mineral), the larger volume of minerals based on X-ray diffraction, risk assessment (fitting parameters), and neutron-sonic porosity cross plot. After these iterative analyses, the final results were calibrated with XRD analyses.

The following sections describe the methods used for TOC and porosity estimation based on log data. We extracted Eqs. (1) and (2) from published articles by Ruyue et al. (2015) and Zhu et al. (2018) and further calibrated with laboratory-measured porosity and TOC on core samples of Well J-2.

3.2.1. Total organic carbon (TOC) content

Ruyue et al. (2015) developed the following equation to estimate the TOC content from well log response for shales of the Lower Cambrian Niutitang Formation, China.

The generalized form of their regression model is,

$$\mathrm{TOC} = a\mathrm{GR} + b\mathrm{U} + c\mathrm{Th} + d\mathrm{K} + x\mathrm{DTP} + y\mathrm{DEN} + z\mathrm{CNL} + m\log R + n, \quad (1)$$

where U is uranium, Th is thorium, K is potassium, DTP is sonic travel time, DEN is density, GR is gamma-ray, CNL is a neutron log, R is resistivity, and a, b, c, d, x, y, z, m, and n are the coefficients determined using multiple regression analysis.

The relationship between calculated TOC by multi-variable regression and measured TOC (from the core) demonstrated good correlation, i.e., good curve fitting with measured values throughout the interval, as shown in Fig. 11.

3.2.2. Porosity

Zhu et al. (2018) used the following equation to determine the total porosity in a shale gas formation and calibrated their results with core data.

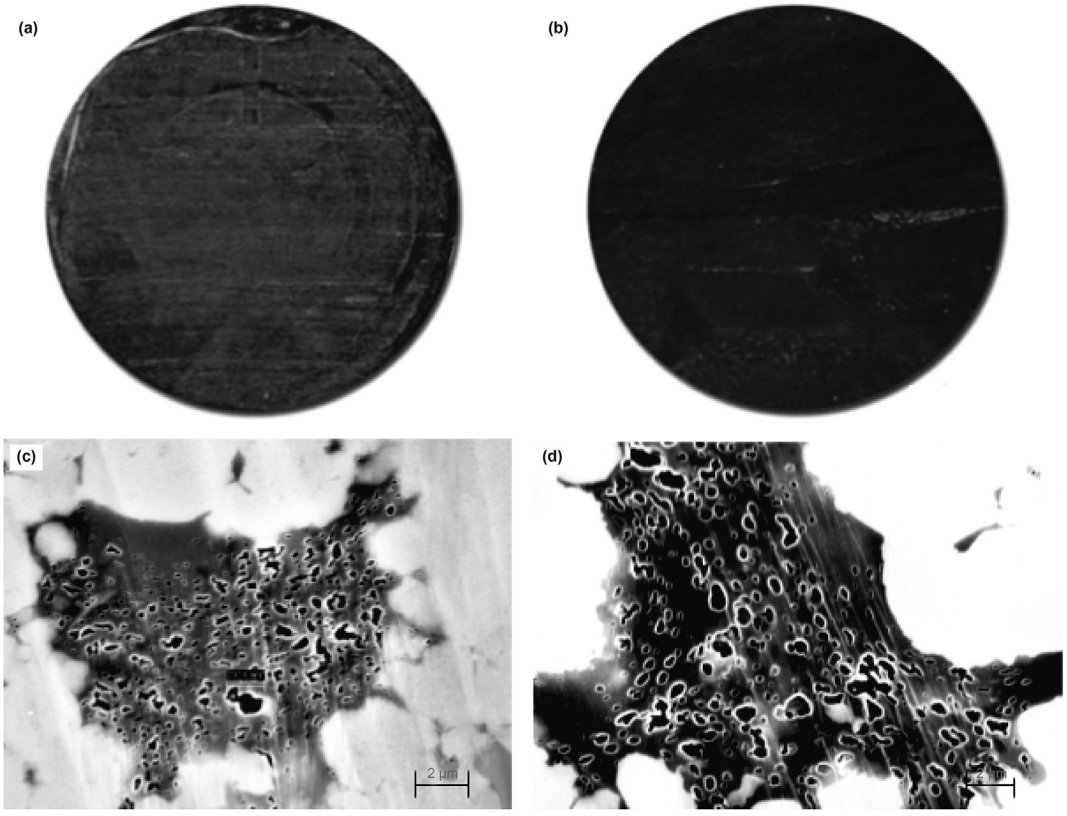

Fig. 2. Images of core samples indicating micro-features and layering. (a) horizontal bedding sample; (b) vertical bedding sample; (c) development of numerous organic pore with diameters up to nanometers; (d) development of organic pore quantity with good connectivity in the Wufeng-Longmaxi Formation.

$$\Phi = \frac{\frac{[(\rho-\rho_{ma})+V_{OM}(\rho_{ma}-\rho_{OM})]}{(\rho_h-\rho_W)} - \frac{[(N-N_{ma})+V_{OM}(N_{ma}-N_{OM})]}{(N_h-N_W)}}{\left[\frac{(\rho_W-\rho_{ma})}{(\rho_h-\rho_W)}\right] - \left[\frac{(N_W-N_{ma})}{(N_h-N_W)}\right]}, \quad (2)$$

where Φ is the total porosity of a shale reservoir in percent; ρ is the density of rock in g/cm^3; ρ_{ma} is rock matrix density in g/cm^3; ρ_{OM} is the density of organic matter in g/cm^3; ρ_W is the density of water in g/cm^3; ρ_h is the density of hydrocarbons in g/cm^3; V_{OM} is the volume percentage of organic matter in percent; N is CNL log response value in percent; N_{ma}, N_{OM}, N_W and N_h are the rock matrix neutron porosity, response value of organic neutron porosity, response value of water neutron porosity, and response value of hydrocarbons neutron porosity, respectively.

3.2.3. Micro-CT scanning

We used a Micro-CT Xradia-400 Versa 3D X-ray microscope to image the microfracture orientation and distribution of minerals in the Longmaxi shale. We acquired the images using 1 mm (diameter) by 3 mm (length) sample for this experiment. The reconstructed images have a resolution of 500 μm. We selected data from the center section of the reconstructed volume with 500 × 500 × 300 pixels. The acquired image data was based on the differential absorption of X-rays and grayscale images with a bimodal population: one mode corresponding to the signal from the void space and the second signal from the matrix. We identified the high-density mineral components within the grayscale images by thresholding segmentation using the Multi-Otsu method, which divides the grayscale histogram into "N" classes by multiple thresholds. The optimal segmentation threshold can be obtained when the inter-class variance of the segmented N groups of data is the largest. The standard operating procedure to capture the microfractures and matrix components' spatial distribution has been discussed in the literature (Jiang et al., 2020).

3.3. UCS (uniaxial compressive strength) test

Destructive testing for UCS estimation was carried out by ASTM Designation, D6931 (2017b). The sample preparation and testing process are as follow:

a) Prepare test specimens according to ASTM Designation D6931 (ASTM 2017b). Sample dimensions, moisture content, and density were previously recorded.
b) Each specimen's end faces were flattened to 0.02 mm and perpendicular to the specimen axis within 0.250 (0.25 mm in 50 mm) (ASTM 2017b). The capping of the samples was not permitted during the time of testing.
c) Each specimen's sides were smooth to be free from abrupt irregularities and consisting of a straight edge within 0.5 mm over the specimen's total length (ASTM 2017b).
d) The load was imposed on each specimen by applying a constant load rate (18 kg/s) such that failure occurred within 5–10 minutes of loading.
e) For testing the samples (one vertical, one horizontal), strain gauges were fixed along the specimen's sides: 2 gauges for axial strain and 2 for lateral strain readings.
f) As discussed by Hucka and Das (1974), the strain approach was used to measure the BI of the samples. In this approach, the stress-strain curve is divided into an elastic region (point O-A), plastic region (point A-B), and failure point (C), as shown in Fig. 3. From Equ. (3), the ratio of reversible and total

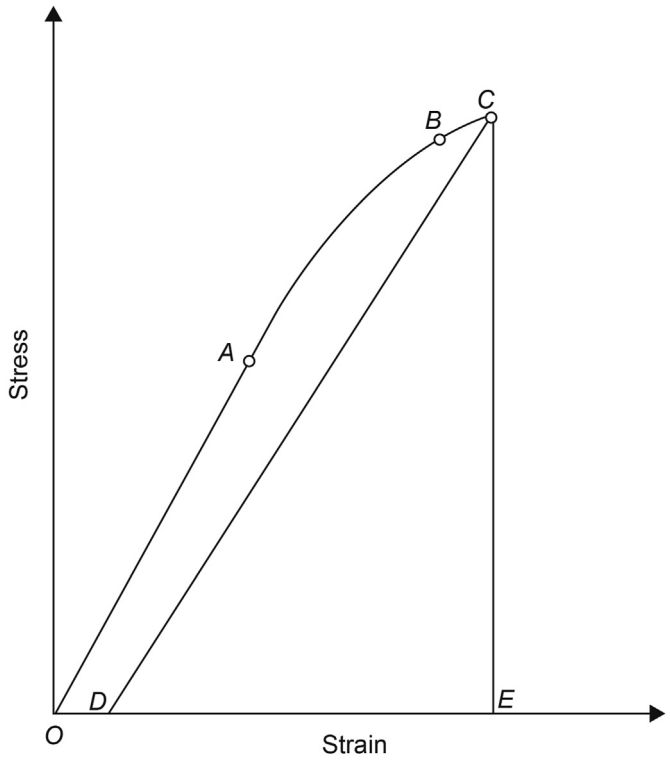

Fig. 3. Determination of brittleness from the stress-strain diagram.

strain was used to measure the brittleness index. The location of point D was determined by assuming that the line CD is parallel to OA.

$$\text{Brittleness Index} = \frac{\text{Reversible strain}}{\text{Total strain}} = \frac{DE}{OE}, \quad (3)$$

4. Results and discussion

4.1. Analysis of petrophysical properties

The overall TOC content in the Longmaxi shale is high, e.g., the TOC values from a total of 20 samples are ranging from 0.2 to 5.6 wt % (Table 3). The TOC content varies with lithofacies, and the highest values takes place in laminated siliceous to argillaceous shale but gradually decreases with increasing the amount of quartz. Liang et al. (2016) reported that the high TOC contents in Longmaxi shale have large gas volumes and high adsorption capacity. The adsorbed gas content in Longmaxi shale ranges from 0.5 to 3.0 m^3/t approximately.

According to the log-core interpretation of Longmaxi shale in the study area, the reservoir characteristics vary from low to medium range, e.g., porosity values from measured core samples range from 3.77 to 7.7%. The permeability of Longmaxi shale is very low, ranging from 0.004 mD to 0.018 mD with an average value of 0.012 mD (Table 3).

The laboratory and log analysis of Longmaxi shale indicate that the mineral content is variable but is dominated by clay minerals and quartz, followed by calcite, dolomite, and pyrite throughout the vertical section. Yasin et al. (2018a) reported that biogenic silicon is dominant at the lower zone of the Wufeng-Longmaxi shale, with a large proportion of organic carbon content has converted to gas production layers. Conversely, the minerals present at the Upper zone were not substantially transformed into organic carbon content due to continental detrital silicon (Li et al., 2016; Liang et al., 2016).

Table 3
Mineral composition, TOC, porosity, and permeability of Longmaxi shale in the Sichuan Basin. (In the table, DEN=density, POR=porosity, and PERM=permeability, note that only specific data are listed because of the space limitation).

Core	DEN	TOC	CLY	QUA	CAL	PYR	POR	PERM
	gm/cc	wt. %	wt. %	wt. %	wt. %	wt. %	%	mD
J-2	2.58	0.7	34.8	38.6	22.6	3.3	3.4	0.007
J-2	2.60	0.3	33.9	36.3	26.5	3.3	3.6	0.007
J-2	2.61	0.5	29.3	36.6	24.2	0.0	3.8	0.007
J-2	2.62	0.6	31.3	37.3	22.1	3.4	3.9	0.009
J-2	2.60	1.0	31.2	38.9	19.1	4.0	7.7	0.008
J-2	2.59	1.6	30.2	38.5	18.5	2.8	6.9	0.011
J-2	2.57	1.5	36.5	42.1	17.7	2.2	6.4	0.007
J-2	2.55	1.7	39.2	38.1	16.6	3.5	6.2	0.006
J-2	2.52	2.2	35.7	42.0	18.4	2.8	6.1	0.005
J-2	2.50	1.6	34.6	43.1	16.7	3.5	6.7	0.008
J-2	2.48	3.8	32.2	44.8	17.3	2.0	7.0	0.005
J-2	2.52	3.2	26.9	38.6	31.3	2.5	5.7	0.004
J-2	2.57	2.5	22.8	36.6	38.1	0.0	5.1	0.012
J-2	2.50	3.5	18.7	32.1	42.0	3.4	6.1	0.014
J-2	2.52	5.6	22.6	32.3	40.7	3.8	5.7	0.015
J-2	2.59	0.9	26.7	42.1	23.5	0.0	6.7	0.018

4.2. UCS test result and correlation analysis

Figs. 4 and 5 show the stress versus strain plots with the samples before and after the test. We utilize the data plotted at 50% of UCS, as indicated by the dashed line on both figures, to determine static elastic moduli and Poisson's ratio. The distortion in data after 100 MPa in Figs. 4 and 5 is due to the breakage of the strain gauges, and we did not consider it in the interpretation of static elastic properties.

The brittleness indices for the vertical (2V) and horizontal samples (4H) (Table 4) are consistent with the broken samples (Figs. 4 and 5). Note that we collected the rest of the data in Table 4 from the China University of Petroleum's uniaxial test laboratory. The laboratory analysis shows no significant difference in the elastic moduli of vertical and horizontal samples. The BI values are quite similar in all samples. However, UCS values are not consistent, and the lowest values may be due to the micro-cracks in the samples. Note that the mechanical BIs are consistent with mineralogy as given in Tables 4 and i.e., high quartz and dolomite seem to play a vital role in defining the sample's strength.

We analyzed the correlation between mineralogy-based BI (i.e., BI defined by Jin et al., 2014 in Table 1) and mechanical-based BI determined by strain approach (as given in Table 4) and established the significance of the *R*-value (correlation coefficient) between the two brittleness indices by *t*-test (Fig. 6). Neter et al. (1988) discussed the *t*-test between two variables using the null hypothesis. According to their study, the *R*-value would be significant if the calculated value of the *t*-value is larger than the tabulated value (t_c), and the null hypothesis is rejected. Fig. 6 shows that the computed *t*-value is less than the tabulated t_c value. This suggests that the correlation between mineralogy-based BI and mechanical BI is not statistically significant. The data depicted in Fig. 6 is highly scattered, and we cannot discern a linear relationship between mineralogy-based BI and the mechanical BI. The reliability of this correlation testing is low. Thus, the use of the traditional mineralogy-based BI in Longmaxi shale is unreliable.

4.3. Improved BI evaluation model

The majority of the recent engineering literature quantify the BI

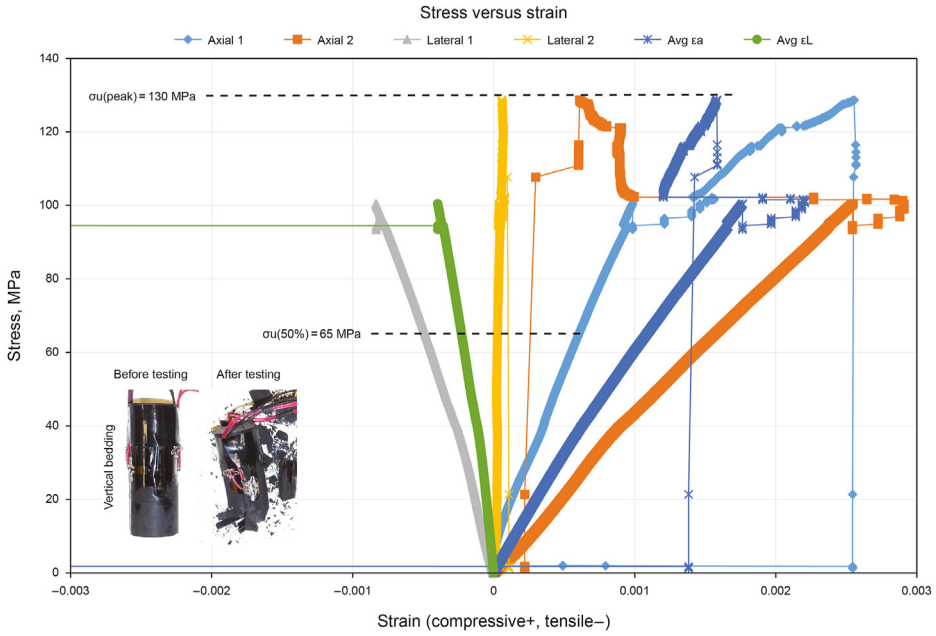

Fig. 4. Stress versus strain curves for the vertical sample (2V).

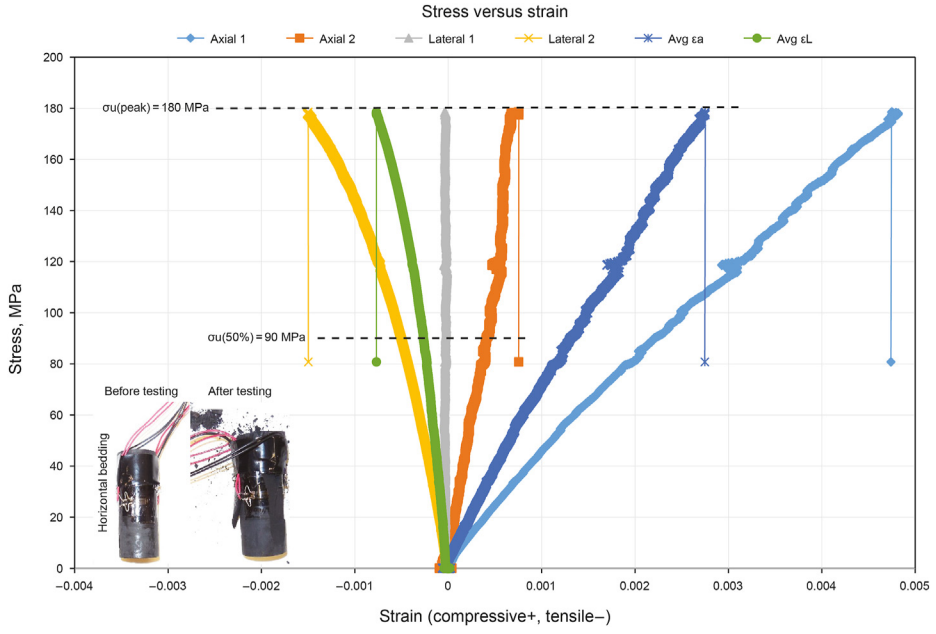

Fig. 5. Stress versus strain curves for the horizontal sample (4H).

with various schemes of rock composition by using a ratio of the weight or volume fraction of minerals more prone to brittle fractures to those less prone to brittle fractures (Grieser and Bray, 2007; Jarvie et al., 2007; Rickman et al., 2008; Wang and Gale, 2009; Sone and Zoback, 2013; Jin et al., 2014). The Wufeng–Longmaxi shale's mineral components are characterized by a relatively high carbonate content in the Lower zone due to the depositional environment. The maximum carbonate content reaches 90% in the Weiyuan region (Zhang et al., 2017). Also, there is a high content of pyrite present in some localized areas. These analyses reveal a complex range of mineral composition in the Longmaxi shale. Therefore, traditional BI methods cannot be applied to evaluate brittleness in the Longmaxi shale.

Based on previous work (Sharma et al., 2017; Huo et al., 2018) and experimental results on the Longmaxi shale gas reservoir, it is evident that the traditional BI model is not appropriate in high calcite content zones and contradicts with proposed brittleness templates for fracability evaluation (the plots are shown in section 6). The results also show low values in TOC-rich zones.

Moreover, a literature study on various shale reservoirs reported that 30 to 40 wt% of calcite content enhances the brittleness's efficiency (Zou, 2011; Weicht, 2015; Sharma et al., 2017). The calcite content above this value may act as a fracture barrier (Sharma et al., 2017; Huo et al., 2018). According to Huo et al. (2018), the

Table 4
Summary of measured geomechanical parameters, mineralogy (from XRD analysis) and total organic carbon (TOC), E: Young's modulus (from compressive strength test), ν: Poisson's ratio, Q=Quartz, CLY=Clay, CAL, Calcite, PYR=Pyrite, FSPR=Feldspar, BI (Mec.)=Brittleness Index Mechanical, BI (Min.)=Brittleness Index from Jin et al., (2014).

Core No.	L. mm	Dia. mm	E GPa	ν ratio	UCS MPa	BI (Mec)	QUA Wt.%	CLY Wt.%	CAL Wt.%	DOL Wt.%	PYR Wt.%	FSPR Wt.%	TOC Wt.%	BI (Min)
1V[a]	54.6	24.8	16.80	0.13	176	0.61	17.4	10.8	28.6	36.6	3.0	2.2	3.4	0.78
2V	61.8	25.2	22.05	0.12	175	0.80	34.	11.8	42.4	08.4	2.2	0.0	3.9	0.81
3V[a]	54.8	24.6	12.15	0.12	118	0.48	28.5	12.1	28.1	24.9	2.9	1.6	3.8	0.79
4V[a]	54.3	24.7	15.95	0.12	208	0.59	58.3	11.2	16.8	06.8	2.3	3.2	3.9	0.81
5V[a]	54.7	24.9	26.22	0.32	186	0.58	24.6	18.4	40.3	08.3	1.0	2.7	4.0	0.84
1H[a]	61.0	24.9	16.02	0.18	145	0.53	19.4	09.8	29.6	34.6	2.0	2.2	3.4	0.85
2H[a]	61.6	24.9	12.95	0.11	149	0.52	36.2	10.8	41.4	07.4	2.2	1.4	3.2	0.84
3H[a]	61.8	24.84	17.52	0.16	190	0.38	30.5	11.0	31.2	22.7	2.9	1.6	3.8	0.83
4H	61.8	25.04	22.95	0.11	235	0.82	59.2	11.2	16.8	08.1	2.1	2.2	3.9	0.84
5H[a]	61.6	24.88	19.00	0.42	122	0.22	26.1	16.4	41.0	11.3	3.0	2.1	4.0	0.75

[a] Data was collected from the uniaxial test laboratory of China University of Petroleum.

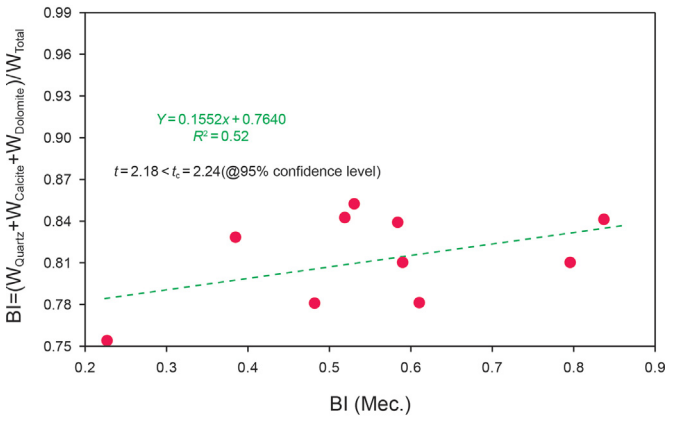

Fig. 6. Correlation between mineralogy-based BI (Jin et al. BI) and mechanical BI (BI_Mec.) (The values are shown in Table 4).

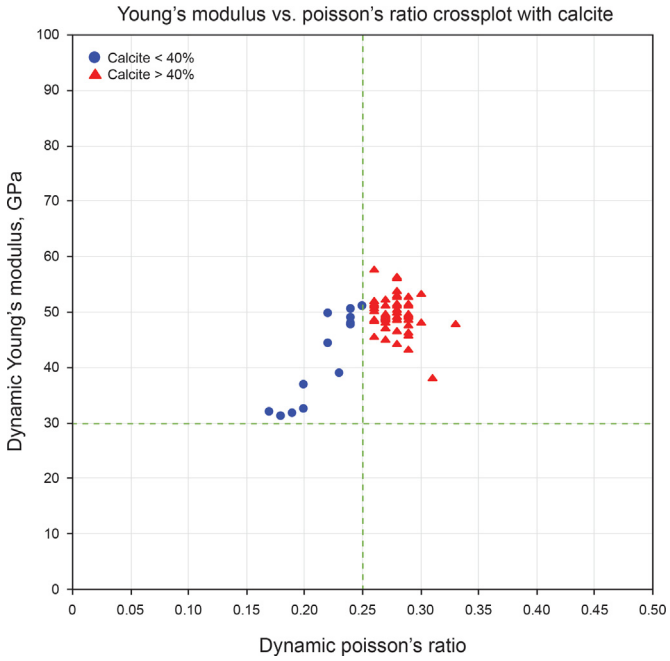

Fig. 7. Cross-plot of dynamic Young's modulus and Poisson's ratio with the composition of calcite minerals in Wufeng-Longmaxi shale.

limestone's brittleness and fracability are low in shale from the Southern North China Basin. They also reported that Young's moduli of the limestones are lower than shales with similar Poisson's ratios. McGinnis et al. (2017), Huo et al. (2018), and Yasin et al. (2021b) reported that the upper (roof) and lower (floor) beds of limestones serve as fracture barriers to restrict the extension of the shale fractures into multiple fracture networks.

Mavko (2008), Sone and Zoback (2013), and Zou (2011) established the relationship between Young's modulus and Poisson's ratio with varying mineralogical composition on various shale gas-producing reservoirs in North America and China. They reported that Young's modulus >30 GPa and Poisson's ratio <0.25 can be taken as standard elastic parameters for brittle mineral definition. Based on these studies, we extracted the zones of Longmaxi shale in multiple wells of the study area with high and low calcite contents, i.e., 30 < calcite <40 in wt. %, and calculated the dynamic Young's modulus and Poisson's ratio for these intervals. Fig. 7 shows that intervals with low calcite <40 wt % is confined in the range of Young's modulus >30 GPa and Poisson's ratio <0.25. On the contrary, the zones/intervals with high calcite >40 wt % have Poisson's ratios >0.25 following Young's modulus >30 GPa. These results show a positive correlation between the amount of calcite and the brittleness of the studied interval.

The analysis also shows that pyrite has a negligible impact on dynamic elastic properties due to its low content (Fjaer et al., 2008; Rybacki et al. 2015, 2016). The general classification of pyrite minerals is that their hardness is equal to quartz and can be considered brittle minerals (e.g., pyrite chemical formula is FeS_2, tenacity is brittle, and hardness on Mohs-scale is 6–6.5) (Hurlbut and Klein, 1985).

Fig. 8 shows the images from micro-CT scanning to study the plane distribution characteristics and connectivity of the microfractures with high-density minerals, i.e., pyrite in the Longmaxi shale. Fig. 8 (a-d) displays the original images from samples 1H and 5V and overlays the microfractures on the original images. The superimposition of microfractures and pyrite minerals shows a good correlation with excellent general spatial connectivity (Fig. 8e and f). We observe that most microfractures are tied with the distribution of pyrite minerals, while some are isolated with a good correlation to matrix components (Fig. 8e and f). It is important to note that the microfractures, connected with the distribution of pyrite mineral, are elongated strips curves of 30–200 μm fracture lengths and 10–80 μm of fracture widths (Gou and Xua 2019).

The possible positions and orientations of microfractures are segmented to highlight micro-crack and pore features in the shale sample (Fig. 9a). We then extend these features along local orientations by modeling the possible paths of deformation features in the segmented images using MIPAR (image analysis software) (Fig. 9b). In Fig. 9c, we show that the microfractures are closely allied with the pyrite mineral distribution. Surprisingly, the

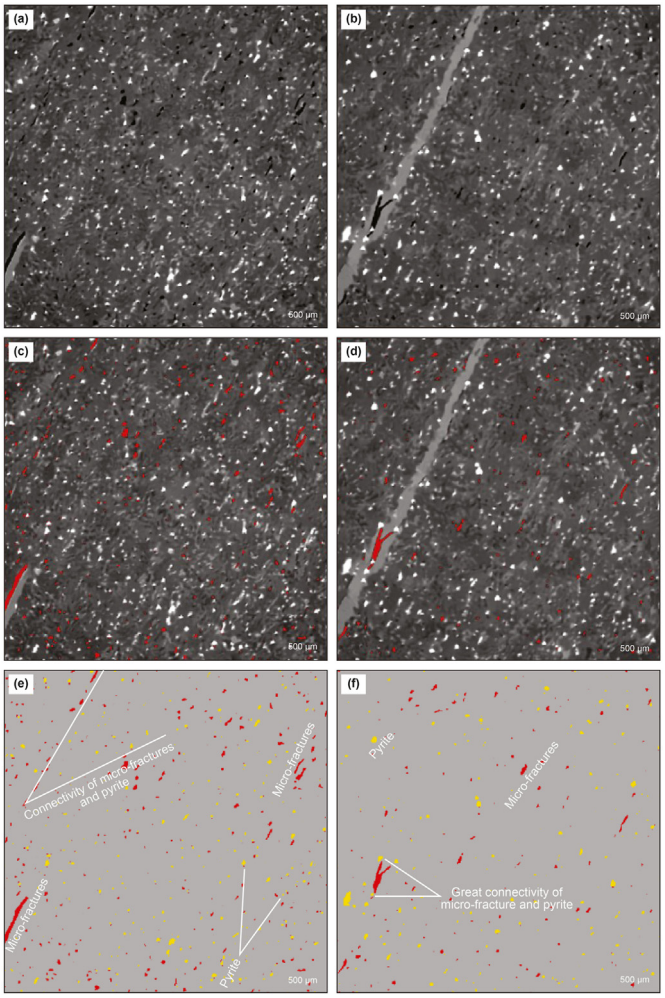

Fig. 8. 2D distribution of minerals (pyrite in vol. %) and microfractures. (a) and (b) original images at different angles; (c) and (d) original images with microfractures; (e) and (f) spatial distribution of pyrite minerals and microfractures. The red color specifies the microfractures, the gray for matrix minerals, and the yellow for the high-density pyrite mineral.

development of microfractures coincides with the uniform distribution of pyrite particles (shown with yellow). This phenomenon changes the mechanical properties of the shale surrounding the mineral, i.e., more pyrite increases Young's modulus and decreases the Poisson ratio determining microfractures under stress (Guo et al., 2019). Therefore, the microfractures connect with pyrite minerals with excellent general connectivity.

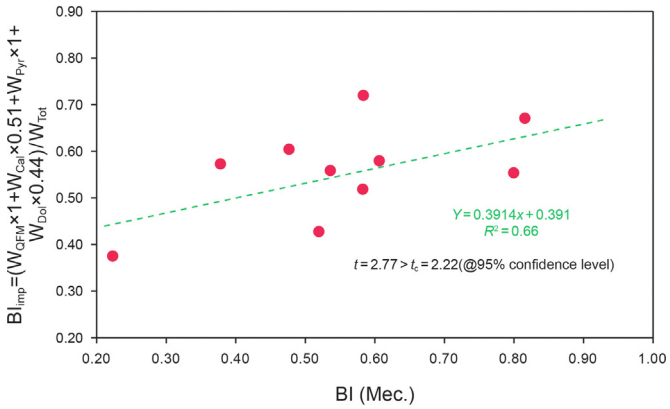

Fig. 10. Correlation between improved mineralogy-based BI and mechanical BI (BI_Mec.).

Based on the comprehensive laboratory experiment, local mineral composition, and elastic properties, we suggest a new brittleness expression by incorporating pyrite as the most brittle mineral. The improved BI model is shown in Eq. (4):

$$BI_{\text{improved}} = \frac{W_{\text{QFM}} + W_{\text{Calcite}} + W_{\text{Dolomite}} + W_{\text{Pyrite}}}{W_{\text{Total}}}, \quad (4)$$

where W_{QFM} is the weight of quartz, feldspar, and mica, W_{Calcite} for the weight-percent of calcite, W_{Dolomite} for the weight-percent of dolomite, W_{Total} for total minerals in wt. % and W_{Pyrite} is a weight fraction of pyrite mineral, $BI_{\text{improved}}=1$ and $BI_{\text{improved}}=0$ indicate brittle and ductile rocks, respectively.

We earlier mentioned that the Wufeng–Longmaxi shale's carbonate content is relatively high in the Weiyuan region. Also, the high calcite contents act as a barrier to stimulation. It is, therefore, necessary to differentiate quartz, calcite, dolomite, and pyrite based on unit weight contribution. According to Fjaer et al. (2008), the quartz's bulk modulus is very low compared to calcite and dolomite. Thus quartz is more brittle. Based on the bulk modulus, the weighting coefficients of quartz, calcite, dolomite, and pyrite are assigned in Eq. (4), as Kang et al. (2020) proposed. Note that the weighting coefficient of pyrite is arbitrarily set to be 1. We write Eq. (5) as:

$$BI_{\text{improved}} = \frac{W_{\text{QFM}}\times1 + W_{\text{Calcite}}\times0.51 + W_{\text{Dolomite}}\times0.44 + W_{\text{Pyrite}}\times1}{W_{\text{Total}}}, \quad (5)$$

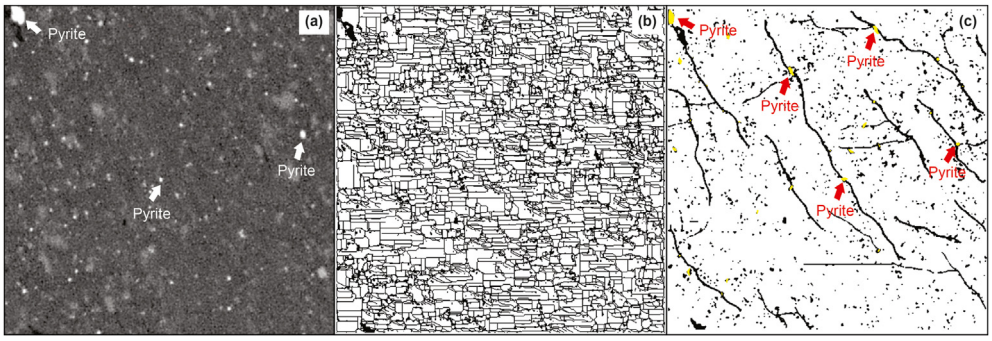

Fig. 9. 2D samples of the Longmaxi shale: (a) original micro-CT images; (b) segmented image; (c) micro-fracture network analyzed by deformation features from the segmented images.

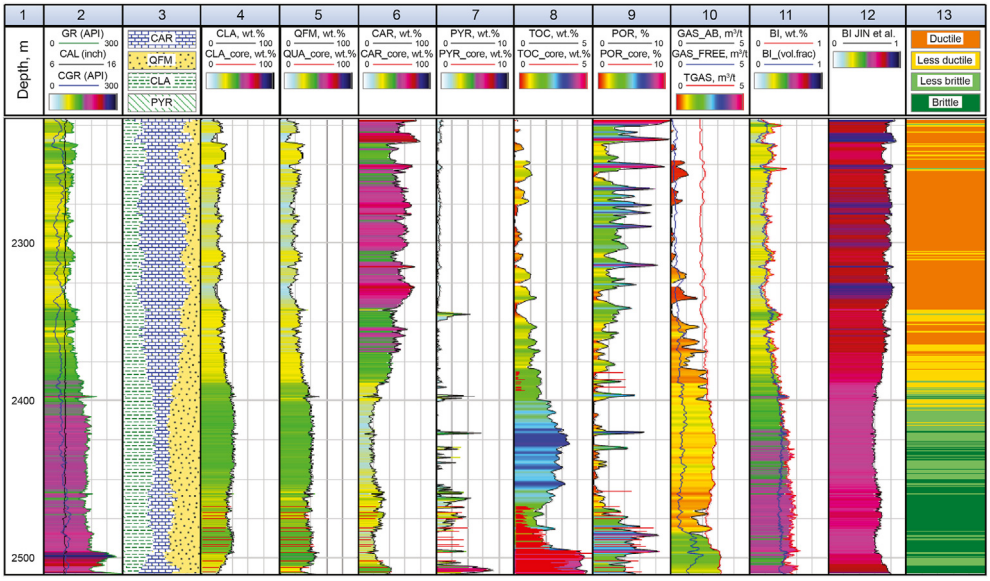

Fig. 11. Log data, core data, and interpreted brittleness indices for Well J-2. Caliper and gamma-ray log (track 2); mineralogical composition in volume fraction (track 3) and weight percentage (tracks 4 to 7 for clay, QFM (quartz, feldspar, and mica), carbonate (calcite and dolomite), and pyrite respectively); petrophysical properties (tracks 8 to 10 for total organic carbon (TOC), POR (porosity), and total gas (adsorbed and free) respectively); improved BI in wt. % and vol. fraction (track 11); BI proposed by Jin et al. (2014) (track 12); and brittle-ductile classification (track 13).

Jarvie et al. (2007), Bruner and Smosna (2011), and Kang et al. (2020) have reported that limestones typically have a higher fracture threshold than the shale and serve as a barrier to fracture growth. From shale to limestone, calcite and dolomite contents increase, and the improved BI decreases because we assigned smaller weighting coefficients to calcite and dolomite minerals compared with the weighting coefficient of quartz and pyrite in Eq. (5). Thus, the improved BI model can be used to identify the limestone barrier.

Fig. 10 shows the correlation between the improved mineralogy-based BI (mineralogy is given in Table 4) and mechanical BI (Table 4). The correlation of the relationship has a statistically significant finding because the computed t-value of 2.77 is larger than this tabulated t_c value of 2.22. It suggests that the improved mineralogy-based BI determined by Eq. (5) is practical and robust for characterizing shale brittleness. Although the correlation between the improved mineralogy-based BI and mechanical BI is not very high, it is statistically significant.

Fig. 11, track 11 (in vol. fraction and wt. %) shows the result of an improved BI evaluation model, while track 12 indicates the traditional BI model profile as proposed by Jin et al. (2014). Though pyrite has more grain density than bulk samples, their fraction decreases when converting from weight percent to volume fraction. So, we estimated the improved BI in both wt. % and vol. fraction to observe the difference. By comparing Jin et al. (2014) and the improved BI definition, we observe that the values are significantly affected by assigning smaller weighting coefficients to calcite. It is important to note that improved BI tends to be high along TOC-rich zones with high adsorbed gas content. Apart from that, the Jin et al. (2014) BI shows higher brittleness values along the non-organic rich zones (Fig. 11, track 12). It is worth noting that the improved BI shows high resolution and better prediction of brittle zones, the petrophysical properties, and elastic parameters (the plots are shown in section 5 to support the statement).

4.4. Influence of TOC, porosity, and mineralogy on improved BI

To investigate the influence of fundamental rock properties on the improved BI, we generate cross-plots of gamma-ray (GR) versus improved BI with TOC content, porosity, and quartz content for the Longmaxi shale in Well J-2. The results indicate that improved BI increases with increasing quartz content and gamma-ray values (Fig. 12a). Porosity shows a non-linear correlation with GR and improved BI (Fig. 12b). Previous engineering literature also suggests that porosity shows nonlinearity with brittleness. As demonstrated in our previous work (Yasin et al., 2018a), TOC and quartz content tend to positively correlate in the Longmaxi shale, indicating a biogenic source of quartz. Subsequently, the other cross-plots reveal a trend of increasing TOC content towards high GR and improved BI (Fig. 12c).

According to the variations of improved BI with fundamental rock properties, the data sample is sorted into four petro-types classifying the BI between 0.10 and 0.20 for ductile (red), between 0.20 and 0.30 for less ductile (golden), between 0.30 and 0.40 for less brittle (blue), and greater than 0.40 for brittle (green) (Fig. 12d). The classification results are shown in Fig. 11, track 13.

Examining the proposed classification of ductile, less ductile, less brittle, and brittle zones, the Lower part of the Longmaxi shale falls into the brittle and less brittle zone due to the high concentration of quartz. In contrast, we observed several thin ductile and less ductile layers in the Upper part of the shale formation due to the high concentration of carbonate and clay contents.

The Lower zone of Longmaxi shale across the brittle region (improved BI > 0.4) exhibits higher TOC, adsorbed gas content, and porosity, e.g., TOC >2%, porosity >6%, and total gas content (adsorbed and free gas) > 3 m^3/t (Fig. 11). The biogenic source of quartz at the Lower zone of the Longmaxi shale is consistent with the high carbon content and gas production layers (Zhu et al., 2019).

5. Calibration of common rock constitution to geomechanical properties

5.1. Young's modulus versus Poisson's ratio

Based on the fundamental rock properties as determined by laboratory testing and specific logging data, and improved BI, we create a simple rock model to quantify theoretical values of

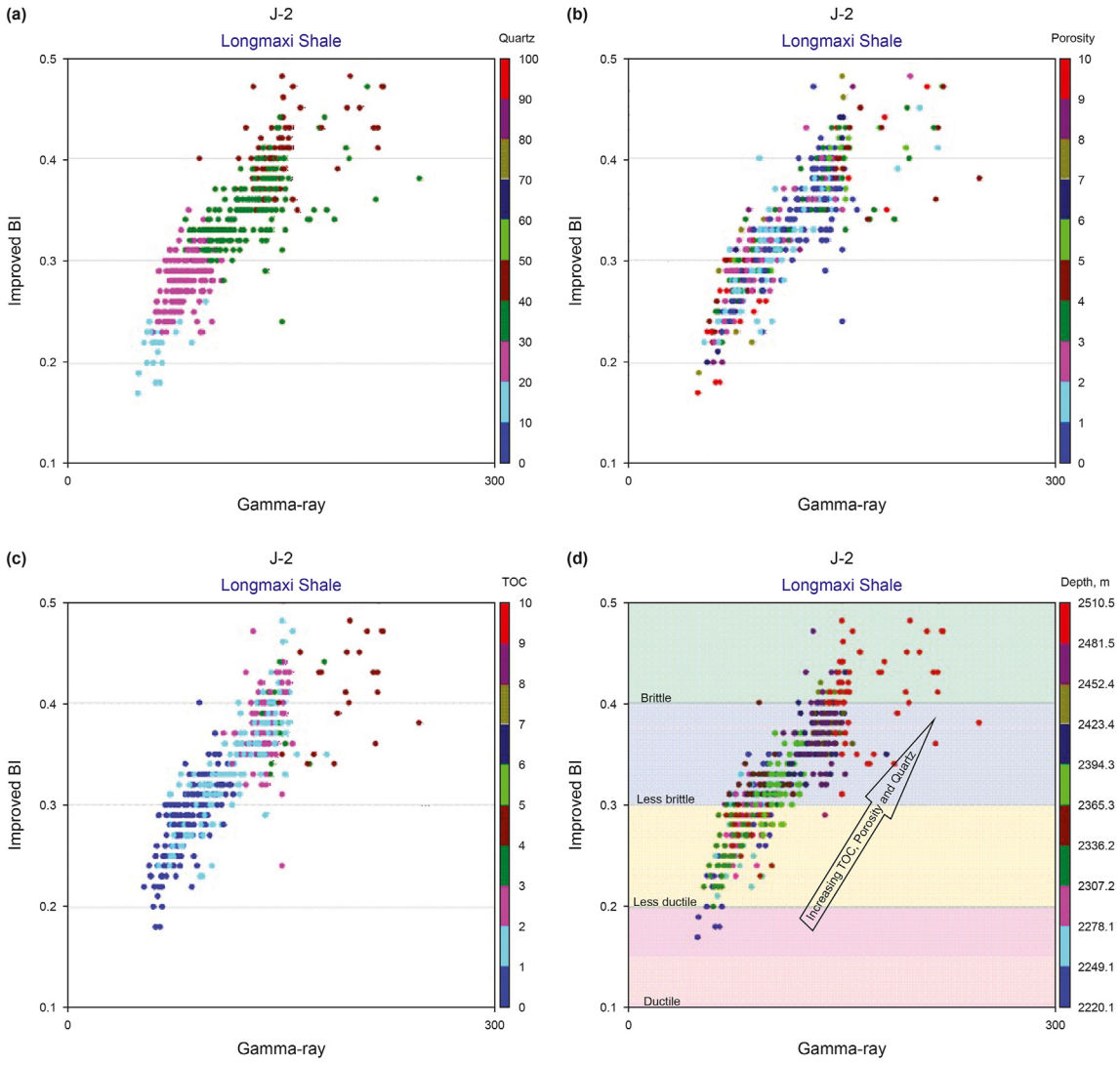

Fig. 12. Improved BI versus GR cross-plots for Well J-2 with colors denoting (a) quartz content (wt. %); (b) Porosity; (c) TOC; (d) proposed classification as brittle (green), less brittle (blue), less ductile (yellow), and ductile (pink).

dynamic elastic properties for a common rock constitution (mineralogy, porosity, TOC, and gas content) for deep learning of brittle and ductile behavior in Longmaxi shale.

Fig. 13 shows a cross-plot of Young's modulus versus Poisson's ratio overlaid with fundamental rock properties. Such schemes highlight the variation of dynamic elastic properties with common rock constituents, e.g., a high percentage of quartz shows lower values of Poisson's ratio (<0.25) and moderate values of Young's modulus (20–50 GPa), as shown in Fig. 13a. Jarvie et al. (2007), Wang and Gale (2009), and Jin et al. (2014) reported that the quantity of quartz has a dominant control on rock brittleness. Interestingly, the higher values of TOC content (>2%), porosity (ranging from 2 to 6%), and pore fluid saturation (gas saturation) (>2 m^3/t) (Fig. 13b, c, and d) are confined in the Poisson's ratio range from 0.15 to 0.20 and Young's modulus from 20 to 40 GPa. According to Ding et al. (2012), shale with high TOC and total gas accumulation has well-developed fractures and indirectly is a high brittle zone. Compared to recent studies on Marcellus shale (Weicht, 2015), the Longmaxi shale tends to show a high Young's modulus for low TOC.

The cross-plot of Young's modulus and Poisson's ratio with natural fracture density indicates that higher fracture density intervals generally possess Young's moduli and Poisson's ratios confined to the ranges of 30 GPa–40 GPa and 0.15 to 0.20, respectively (Fig. 14a). Yasin et al. (2018a) and Golsanami et al. (2019) report that brittle rocks typically have higher denser natural fracture densities, and less energy would be required to initiate fracture propagation patterns in such rocks. The description and analysis of natural fractures in the studied wells can be found in our companion paper (Yasin et al., 2018b).

Based on the differences in the values of Young's modulus and Poisson's ratio along with typical rock compositions and natural fractures, we propose four petro-types and an associated brittleness classification (Fig. 14b). The shale with higher values of improved BI (>0.4) tends to fall in the region defined as brittle, and shales with lower values of improved BI (<0.2) fall into the less ductile and ductile regions. The transition between the brittle and ductile region is signified by the variations of quartz minerals (the standard for differentiating brittle and ductile rock) and improved BI (between 0.2 and 0.4) (see Fig. 12d) (Sharma et al., 2017). The results are consistent with the relationship established by Mavko (2008), Zou (2011), and Sone and Zoback (2013) on various gas

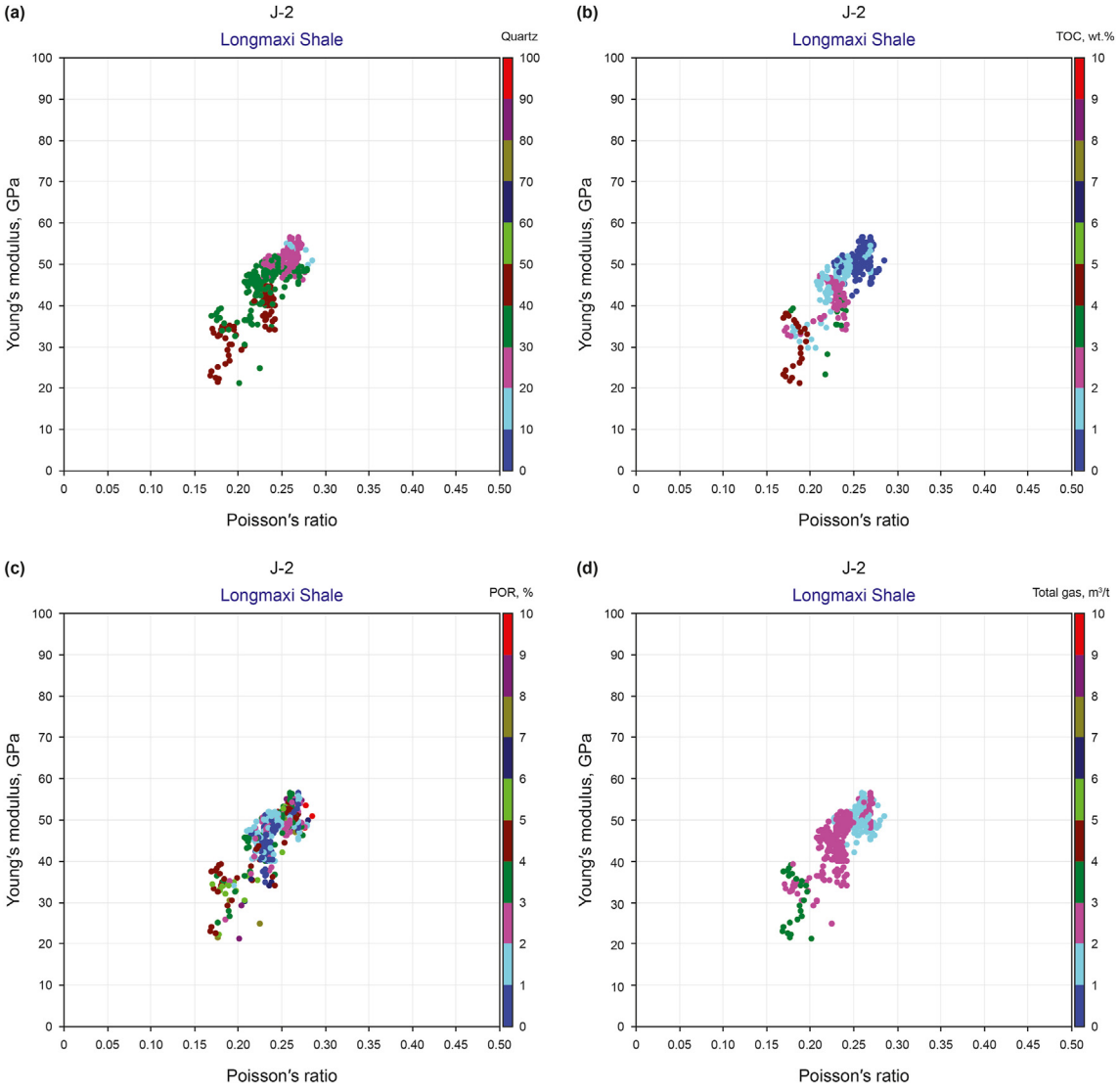

Fig. 13. Young's modulus versus Poisson's ratio cross-plots overlaid to (a) quartz content (wt. %); (b) TOC content; (c) porosity; (d) total gas content.

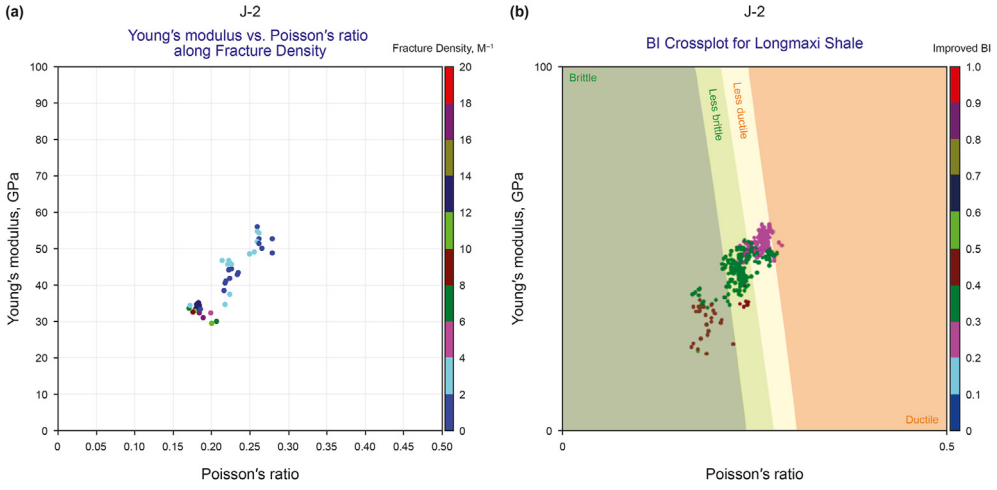

Fig. 14. Young's modulus versus Poisson's ratio cross-plots with colors denoting (a) fracture density; (b) proposed brittleness classification.

production shale reservoirs in the USA, Canada, and China.

To ensure that our results are not unique to this experiment, we correlate different elastic attributes (such as λ, μ, E, and K) with fundamental rock properties to verify the survey-specific brittleness templates.

5.2. The product of λρ versus μρ

Alzate and Devegowda (2013) and Perez and Marfurt (2014, 2015) cross-plotted the product of λρ and μρ to classify fluid discrimination, lithology identification, TOC rich zones, and further correlate the brittleness to reservoir properties in Barnett shale. Taking advantages of their study, we cross-plot the λρ versus μρ to characterize the possible failure features in Longmaxi shale for Well J-2. On the cross-plot of λρ versus μρ overlaid by gamma-ray (Fig. 15a), the associated minerals (quartz, clay, and calcite) in the Longmaxi shale are plotted using their typical moduli and densities.

Notice the differences in rock properties with the variation of the λρ versus μρ; e.g., shale with higher values of GR, TOC content, porosity, and total gas content is confined to lower values of λρ (ranging from 10 to 25 GPa-g/cm^3) and μρ (ranging from 25 to 45 GPa-g/cm^3) (Fig. 15a, b, c, and d). We utilize Lame's parameters (λ and μ) to determine the stiffness, rigidity, and shear modulus of rock, respectively (Perez and Marfurt, 2015). Alzate and Devegowda (2013) recently used λρ and μρ cross-plots to classify the organic-rich zones and brittleness sweet spots. In Fig. 15a, we observed that when clay content increases, μρ and λρ decrease and both increase with an increase of calcite. This observation implies that a λρ and μρ cross-plot could be a good indicator for lithology and brittleness in shale rock. Perez and Marfurt (2015) reported that the lower λρ and the medium to the high μρ region could be considered a brittle region. The result of the cross-plot clusters of λρ versus μρ with gamma-ray, TOC content, porosity, and total gas content, clearly help to evaluate the brittleness and ductility of Longmaxi shale.

Notably, the intervals of high natural fracture density (Fig. 16a) show higher TOC values, e.g., greater than 2% and better-adsorbed gas contents, and also porosity at the lower end of λρ (ranging from 10 to 25 GPa-g/cm^3) and μρ (ranging from 25 to 45 GPa-g/cm^3). Based on the differences in values of the λρ versus μρ along with common rock constitutions and fracture density zones, the authors propose sorting the data into four petro-types with the brittleness classification shown in Fig. 16b. We show that the population of

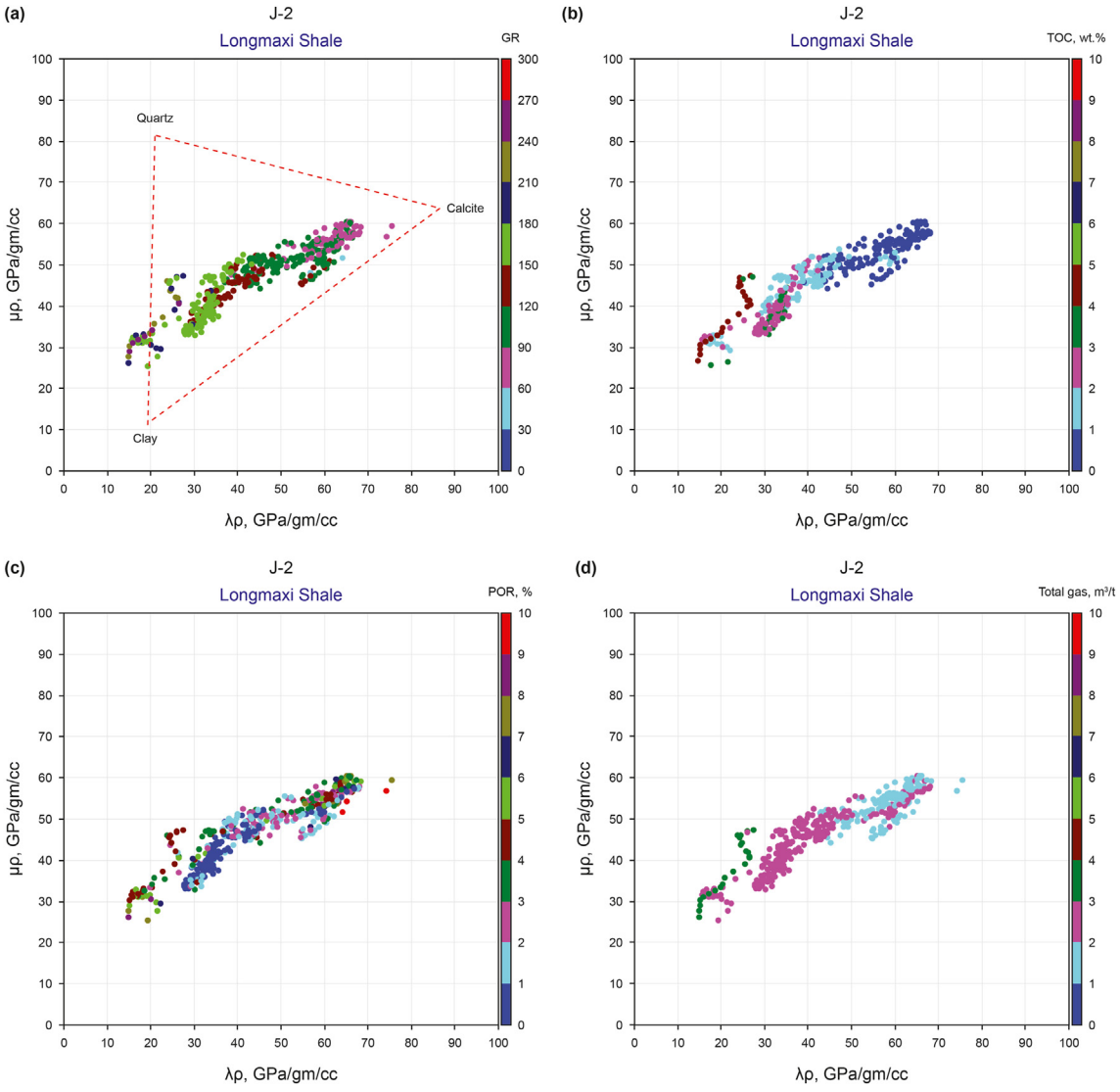

Fig. 15. μρ versus λρ cross-plots. (a) gamma-ray; (b) TOC content; (c) porosity; (d) total gas content.

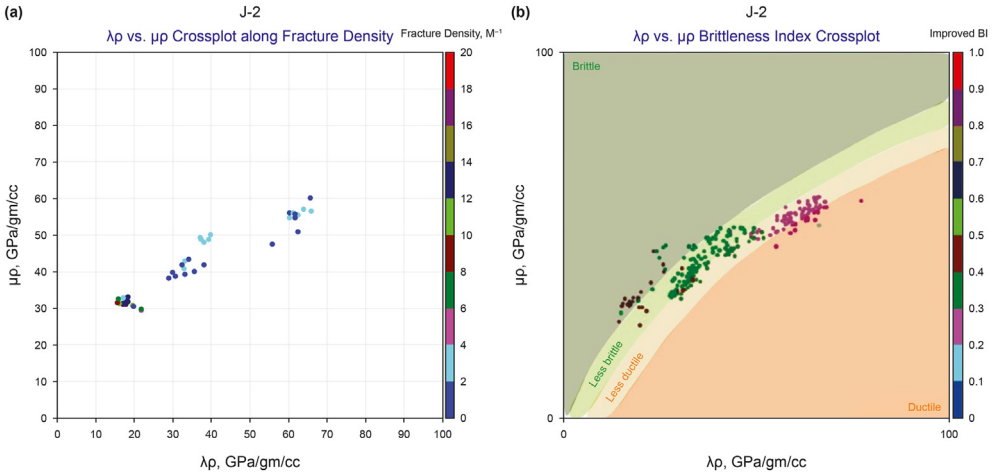

Fig. 16. The μρ versus λρ cross-plots. (a) fracture density; (b) proposed brittleness classification.

data with greater values of improved BI (>0.4) tends to follow the predicted brittle region compared with lower values of improved BI (<0.4) which fall within the predicted less ductile and ductile region. We classify the zones of less brittle and less ductile by the transitional values of limestone and shale identified from gamma-ray log readings and superimpose the associated minerals (quartz, clay, and calcite) in the Longmaxi shale (Fig. 15a).

5.3. The product of Eρ versus Kρ

Taking advantage of other elastic constants, such as shear and bulk moduli, we cross-plot Young's modulus and density in the form of Eρ and bulk modulus and density in the form of Kρ to classify the brittle and ductile nature of Longmaxi shale.

The cross-plots of Eρ versus Kρ with the fracture density suggest that shale with high fracture density zone exhibit high Eρ and low Kρ (Fig. 17a). Sharma and Chopra (2013) indicate that the combination of Young's modulus and density (Eρ) usually gives higher values in brittle rock.

Following the previous approach, we divide the data populations into four petro-types with a proposed brittleness classification based on Eρ and Kρ, as shown in Fig. 17b. Data points with high values of improved BI (>0.4) follow the predicted brittle and less brittle regions, and points with lower values of improved BI (<0.4) gradually fall to the less ductile and ductile regions on the Eρ-Kρ cross-plot.

To determine brittleness laterally, the data from horizontal Well J-2H is used to extract Poisson's ratio, Young's modulus, λ, μ, ρ, and bulk modulus (K) values along the horizontal section of Longmaxi shale and superimposed on the proposed brittleness templates. It is worth mentioning that the aim of using data from the horizontal well is to observe the trend of brittleness horizontally. Here we did not consider the anisotropy components.

The cross-plots of multiple elastic attributes, i.e., Young's modulus versus Poisson's ratio (Fig. 18a), λρ versus μρ (Fig. 18b), and Eρ versus Kρ (Fig. 18c) along with improved BI show that much of high BI data points are gathered in the brittle region and only a few low BI data points likely to fall into the ductile or less ductile region. The results validated the improved BI and proposed brittleness templates, and they are also consistent with BI measured using stress-strain curves of horizontal samples (Figs. 4, 5, and Table 4).

6. Model calibration

We further verify the applicability of the brittleness templates to extract the petrophysical and geomechanical properties for a

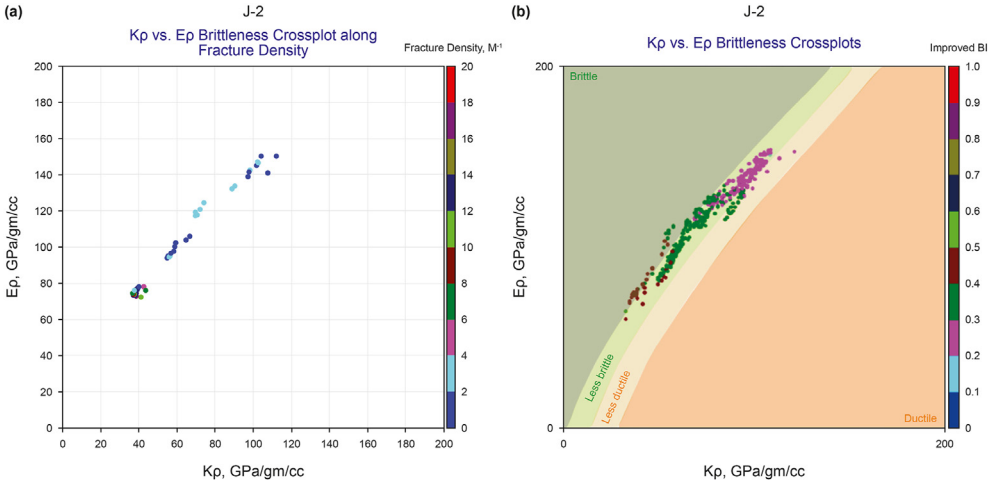

Fig. 17. Eρ versus Kρ cross-plots. (a) fracture density; (b) proposed brittleness classification.

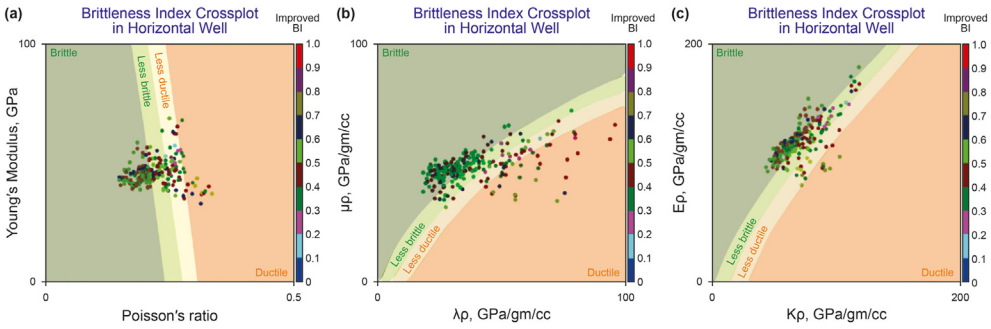

Fig. 18. Cross-plots in a horizontal well. (a) Young's modulus versus Poisson's ratio; (b) λρ versus μρ properties; (c) Eρ versus Kρ with color-coded brittleness index overlaid with proposed BI templates.

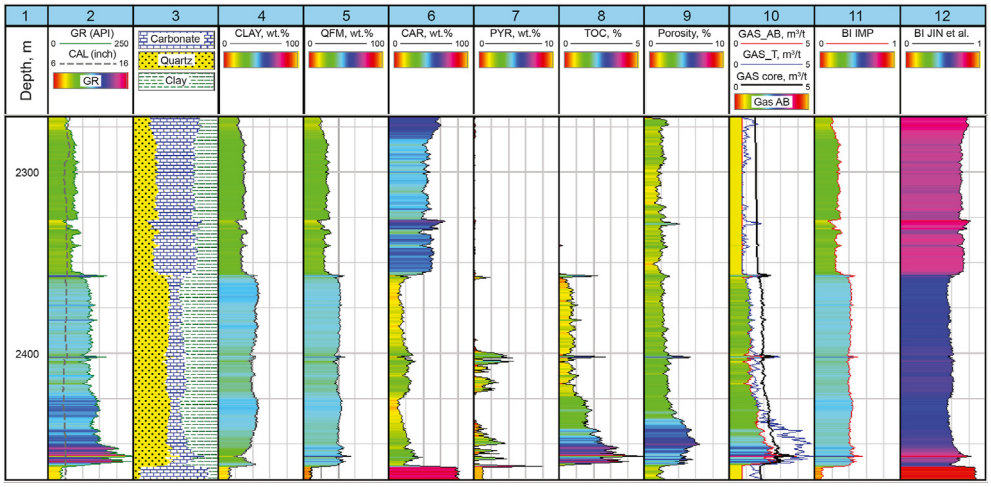

Fig. 19. A set of mineralogical composition in weight percentage (tracks 4 to 7), petrophysical properties (tracks 8 to 10), improved BI from wt. % of minerals (track 11), and BI proposed by Jin et al. (track 12) for the J-3 offset well.

vertical section of Longmaxi shale in an offset well (Well J-3) and superimpose the templates as shown in Fig. 19.

Comparing the improved BI and Jin et al. (2014) BI with the mineralogical composition (Fig. 19, tracks 4–7), we observe that the values are significantly affected by pyrite minerals and the weighting coefficient. Notably, the improved BI shows high resolution and better prediction of brittle zones than Jin et al. (2014) BI (Appendix A shows the plots). We verified the accuracy of the improved BI through elastic parameters and the rock's petrophysical properties.

We observe that the Lower zone of Longmaxi shale in offset Well J-3 exhibits higher TOC, as well as total gas content and porosity, compared to Well J-2, e.g., TOC >3%, porosity >6% and total gas content (adsorbed and free gas) > 4 m^3/t (Fig. 19, track 8, 9, 10).

7. Field application

Brittleness is a complex function of rock strength, lithofacies, mineralogical composition, TOC, stresses, temperature, diagenesis, and porosity. These properties vary from basin to basin. Therefore, it is not easy to predict shale brittleness from a successful model developed for other shales. This section verifies the proposed brittleness templates through data from a shale gas well with slightly different shale compositions. Fig. 20 shows the log interpretation results of Well 106, i.e., the mineralogical composition in wt. % and vol. fraction for the improved (track 11) and Jin et al. (2014) BI values (track 12), and petrophysical parameters (porosity and gas saturation). The separation in the overlapping of shear sonic fast and shear sonic slow suggests a fractured reservoir (track 13). Further, the improved BI values were overlaid with the proposed brittleness templates, as shown in Fig. 21.

The cross-plots of Young's modulus versus Poisson's ratio with improved BI ensure that the high BI data points tend to follow the brittle region as specified in the proposed templates (Fig. 21a). The additional cross-plots of μρ versus λρ (Fig. 21b) and Eρ versus Kρ (Fig. 21c) with the improved BI also confirm the validation of the proposed brittleness template. We show that the high BI data points follow the region specified as brittle and less brittle, whereas the low BI data points tend to follow the ductile and less ductile regions.

8. Quantitative seismic prediction of BI

The improved BI model was used to transform the seismic reflection data into the spatial variability of brittleness over the study area. In this study, we applied the joint inversion strategy based on the multi-layer linear calculator (MLC) and particle swarm optimization (PSO) algorithms to estimate the spatial variations of BI. The theory, method, and workflow of MLC and PSO inversion strategy for predicting reservoir parameters can be found in our previous work (Qiang et al., 2020; Yasin et al. 2020, 2021a; Sohail et al., 2020).

Fig. 22 shows the results when we apply the MLC and PSO inversion strategy to interpret pre-stack seismic data. The inverted BI profile across the Wells 106, J-3, and J-2 shows high-resolution

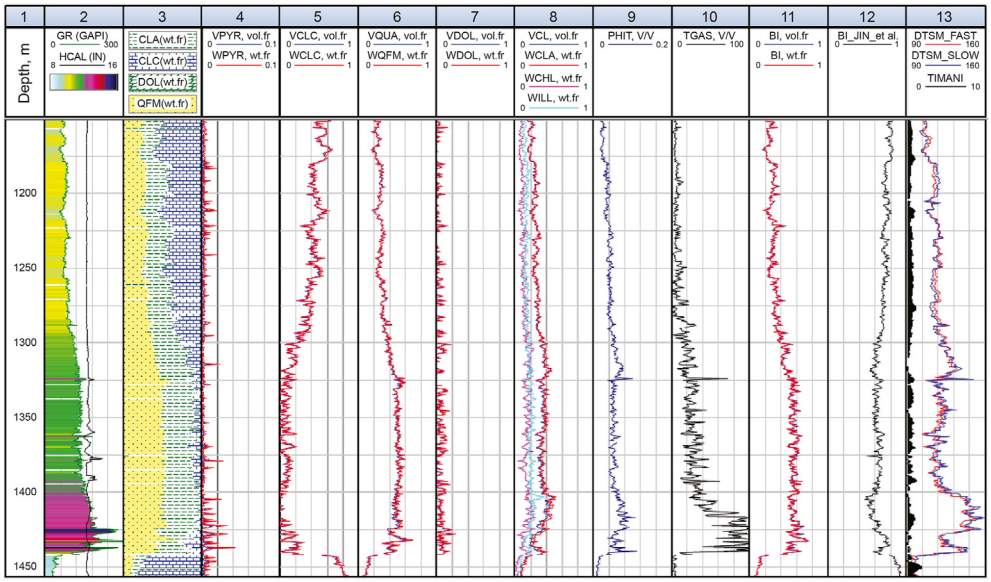

Fig. 20. Set of mineralogical composition (tracks 4 to 7), porosity (track 9), gas saturation (track 10), and improved BI in wt. % and vol. fraction (track 11), BI_Jin et al. (2014) (track 12), and overlapping of shear sonic fast and shear sonic slow (track 13) corresponding to Well 106 from a shale gas reservoir.

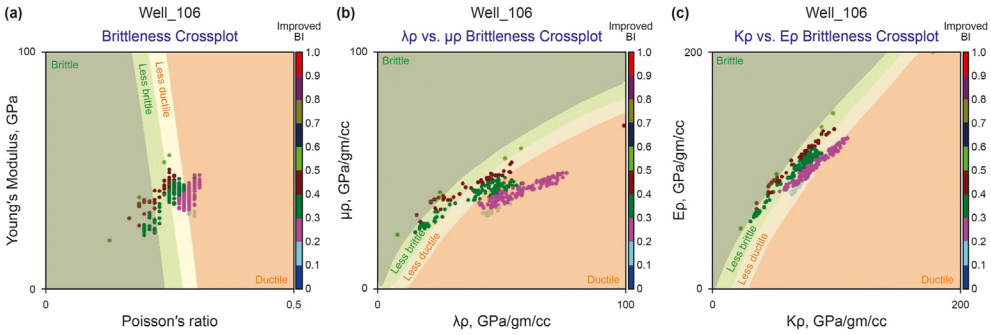

Fig. 21. (a) Poisson's ratio versus Young's modulus; (b) μρ versus λρ; (c) Eρ versus Kρ brittleness cross-plots overlaid with the proposed brittle/ductile templates for Well 106.

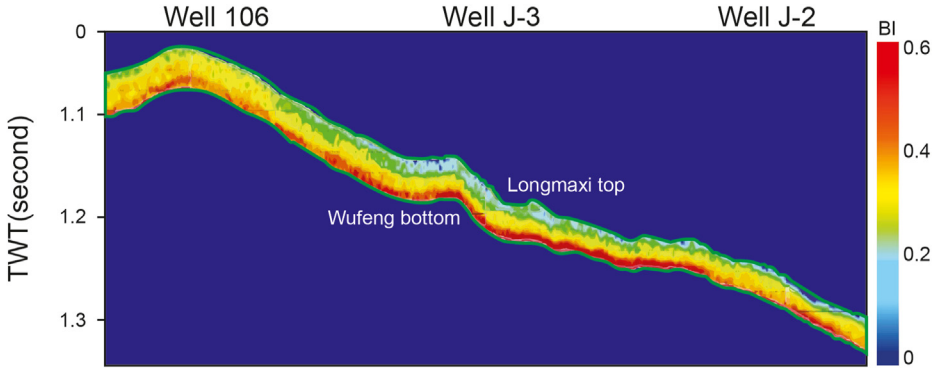

Fig. 22. An inversion profile of BI across the Wells 106, J-3, and J-2.

zonal features longitudinally. We observe that the bottom part of Wufeng–Longmaxi shale has high BI, i.e., 0.4 to 0.6, and corresponds to better fracability and prospective zone for exploration and development. The fracture density data from studied wells verified the reliability of BI prediction results, as shown in Fig. 23. We should note that the brittleness increases downward (towards the depression of the study area), which is consistent with the observations of Li and Li (2018). Furthermore, the BI correlates well with the brittleness indices measured from well logs (Figs. 11, 19, 20) and stress-strain curves in the reservoir interval (Table 4) and brittleness templates.

We generate a time slice of BI to further interpret brittleness distribution over the study area, as shown in Fig. 23a. We observe that the inverted BI surrounding Well 106, Well J-2, and Well J-3 is

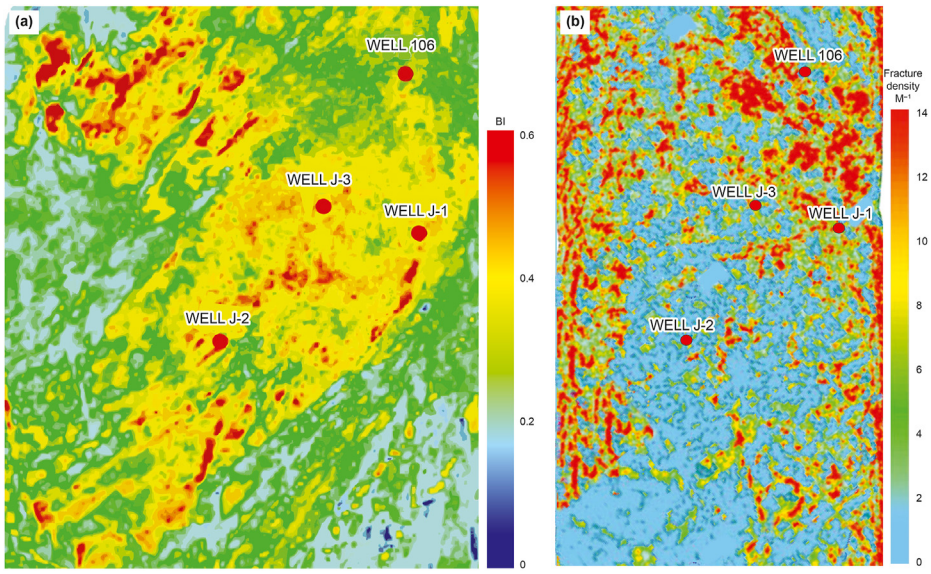

Fig. 23. (a) Inversion slice of BI; (b) fracture density map of the Wufeng-Longmaxi shale in the study area.

relatively high, which indicates a stable distribution and high fracability of shale to produce gas. Fig. 23b shows a fracture density map of the study area that matches well with the inverted BI, verifying the most favorable horizontal drilling and fracturing zone.

9. Conclusions

We constructed the brittleness templates by correlating fundamental rock properties (e.g., mineralogy, porosity, TOC, gas content), improved BI definition, and geomechanical characterization for classifying the brittle and ductile nature of Longmaxi shale using specialized logging tools.

1. The brittleness templates that combine fundamental rock properties, improved BI model, and geomechanical characterization led to high resolution and qualitative assessment of brittleness compared with a stand-alone composition or elastic moduli-based-BI. Good agreement of elastic parameters and fundamental rock properties with predicted brittle regions enhances our confidence for classifying the possible mechanism of failure of the rock mass and characterizing the shale gas reservoir.
2. Overlaying the extracted data from the horizontal well, offset well, shale gas well from a different location within the Sichuan Basin with varying shale composition, and laboratory measurements on core samples to the proposed brittleness templates confirmed the applicability of proposed templates for the evaluation of brittleness. One must keep in mind that exploring shale reservoirs is a highly risky business, and BI plays a crucial role. Therefore geophysical methods with the calibration of laboratory testing are recommended to assess BI for shale gas reservoirs. The seismic inversion profiles of BI across the studied Wells (106, J-3, and J-2) show high BI at the bottom of the Wufeng–Longmaxi shale, which was successfully fractured to produce gas.
3. The improved BI applied to the production well (106) has proved to be valuable for developing the shale gas reservoirs; i.e., the zone of high BI corresponded to the zone of high production rates—from which we infer effective hydraulic fracture development, which in turn suggests brittle behavior of the rock and validate the improved BI.
4. The proposed brittleness templates may be tested in other shale gas formations of China, provided the dominant composition consists of quartz, clay, pyrite, and dolomite. We recommend that petrophysicists overlap the shale samples from their locations on our proposed brittleness templates and correlate them with petrophysical properties to check this approach's reliability.

Acknowledgements

This research is supported by the National Science Foundation of China (41930429 and 41774139), the China National "111" Foreign Experts Introduction Plan for the Deep-Ultradeep Oil & Gas Geophysical Exploration. The rock mechanic laboratory, University of Saskatchewan, Saskatoon, Canada is acknowledged for providing lab facilities and technical support.

Acronyms

TOC	total organic carbon
BI	brittleness index
XRD	X-ray diffraction
ECS	elemental capture spectroscopy
FE-SEM	field emission scanning electron microscopy
E	Young's Modulus
ν	Poisson's ratio
G	Shear Modulus
K	Bulk Modulus
λ	Lame's 1st parameters
μ	Lame's 2nd parameters
GR	gamma-ray
RS	shallow resistivity
RT	deep resistivity
DEN	bulk density
CNL	neutron porosity
DTS	shear sonic
DTP	compressional sonic
PEF	photoelectric effect
FMI	formation micro imager

Appendix A

A1 Model Calibration

Overlaying the extracted data from the BI of Jin et al. (2014) and the improved BI on the template of Young's modulus and Poisson's ratio indicating the points of high BI from Jin et al. (2014) are confined into the less ductile and ductile area (Fig. A1a), generating a conflict with the BI definition. On the other hand, the data points of high BI from the improved model tend to follow the regions specified as more brittle and less brittle, and the data points of low BI follow the regions specified as ductile and less ductile (Fig. A1b).

Subsequently, comparing the templates of other elastic parameters (Lame's parameters (μρ vs. λρ) and product of Eρ vs. Kρ) with the BI of Jin et al. (2014) and the improved BI model verifies the reliability of prediction for the improved BI model and proposed brittleness templates. We show that the data points of high BI from Jin et al. (2014) fall into the ductile and less ductile regions (Figs. A2a and A3a) and the data points of high BI from the improved model fall into the regions defined to be brittle and less brittle (Figs. A2b and A3b).

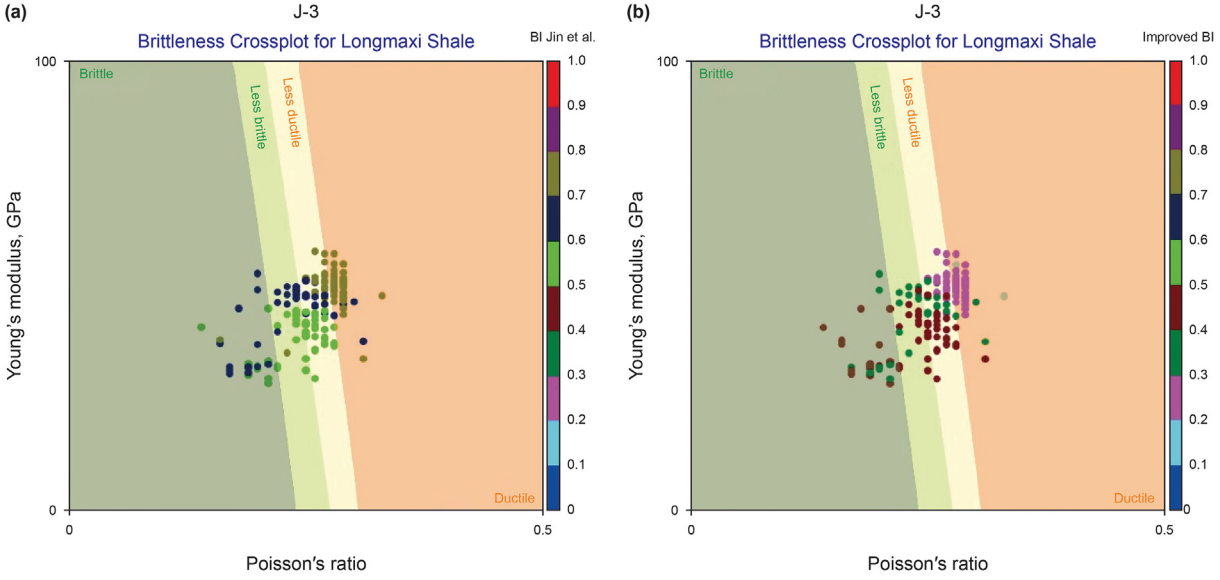

Fig. A1. (a) overlaying of Jin et al. (2014) BI and (b) overlaying improved BI on the proposed template based on Young's modulus and Poisson's ratio for Well J-3.

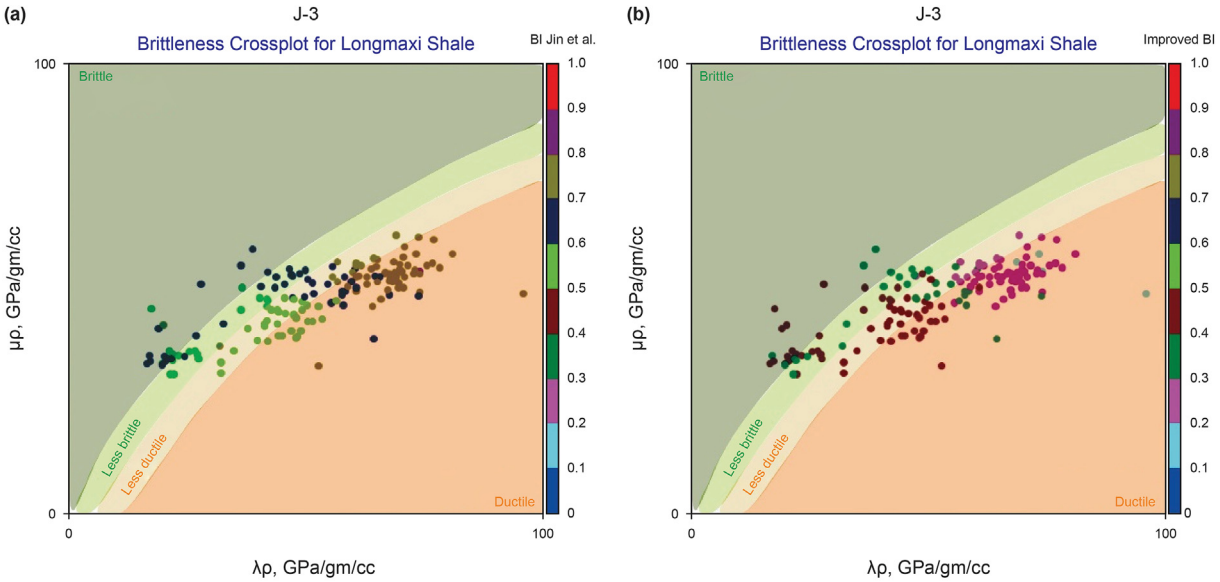

Fig. A2. μρ vs. λρ cross-plots (a) with color-coded BI of Jin et al. (2014), and (b) color-coded improved BI overlaid on the proposed template for Well J-3.

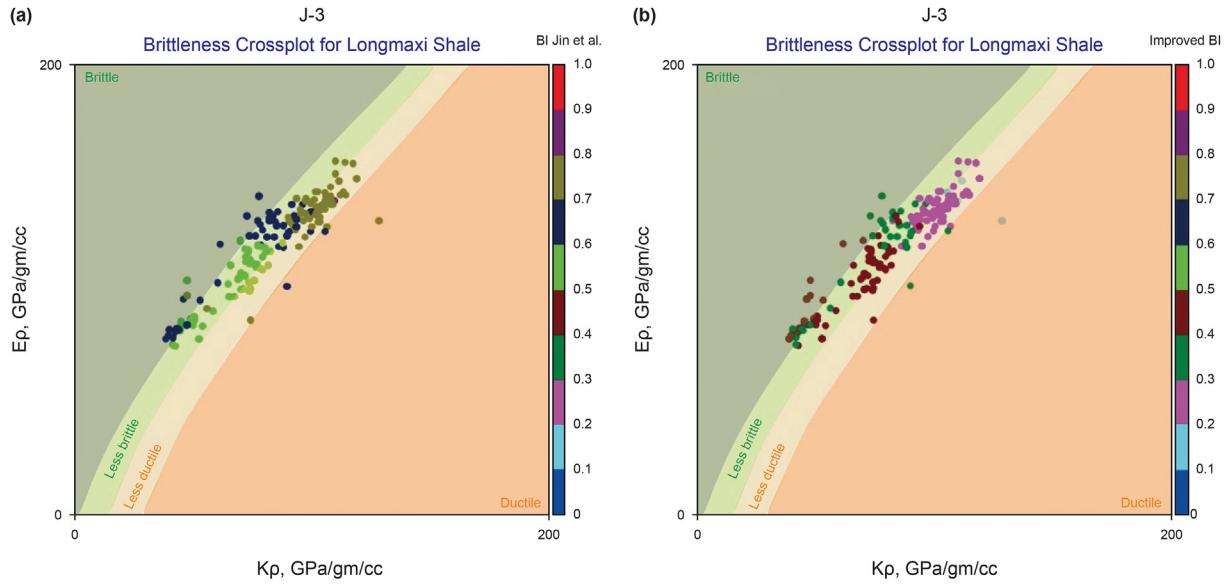

Fig. A3. Eρ vs. Kρ cross-plots (a) with color-coded BI of Jin et al. (2014), and (b) color-coded improved BI overlaid on the proposed template for Well J-3.

References

Altindag, R., 2003. Correlation of specific energy with rock brittleness concepts on rock cutting. J. S. Afr. Inst. Min. Metall 103, 163–171.

Alzate, B., Devegowda, D., 2013. Integration of surface seismic, microseismic and production logs for shale gas characterization: methodology and field applications. Interpretation 1. SB37–SB49.

Amir, M., Nejad Robert, F., Shelley, L., Lehman, et al., 2013. Development of a brittle shale fracture network model. In: SPE Hydraulic Fracturing Technology Conference. The Woodlands, Texas, USA (Extended Abstracts).

Astm, 2017b. Standard Test Method for Indirect Tensile (IDT) Strength of Asphalt Mixtures. ASTM, West Conshohocken, PA.. ASTM D6931.

Bruner, K.R., Smosna, R.A., 2011. Comparative study of the Mississippian Barnett shale, fort worth basin, and Devonian Marcellus shale, Appalachian basin. Natl. Energy Technol. Labo. Rep. DOE/NETL-2011/1478.

Dai, J., Zou, C., Liao, S., et al., 2014. Geochemistry of the extremely high thermal maturity Longmaxi shale gas, southern Sichuan basin. Org. Geochem. 74, 3–12.

Diao, H., 2013. Rock mechanical properties and brittleness evaluation of shale reservoir. Acta Petrol. Sin. 29 (9), 3300–3306.

Ding, W., Li, C., Li, C., Xu, C., Jiu, K., Zeng, W., 2012. Fracture development in shale and its relationship to gas accumulation. Geoscience Frontiers 3 (1), 97–105.

Fjaer, E., Holt, R.M., Horsrud, P., Raaen, A.M., Risnes, R., 2008. Petroleum Related Rock Mechanics, 53. Elsevier, pp. 251–287.

Golsanami, N., Sun, J., Liu, Y., Yan, W., et al., 2019. Distinguishing fractures from matrix pores based on the practical application of rock physics inversion and NMR data: a case study from an unconventional coal reservoir in China. J. Nat. Gas Sci. Eng. 65, 145–167.

Goodway, B., Perez, M., Varsek, J., et al., 2010. Seismic petrophysics and isotropic-anisotropic avo methods for unconventional gas exploration. Lead. Edge 29, 1500–1508.

Gou, Q., Xua, S., et al., 2019. Full-scale pores and micro-fractures characterization using FE-SEM, gas adsorption, nano-CT and micro-CT: a case study of the Silurian Longmaxi Formation shale in the Fuling area, Sichuan Basin, China. Fuel 253, 167–179.

Grieser, B., Bray, J., 2007. Identification of production potential in unconventional reservoirs. In: Production and Operations Symposium of Society of Petroleum Engineering (SPE). SPE-106623-MS.

Guo, Z., Li, X., Liu, C., et al., 2013. A shale rock physics model for analysis of brittleness index, mineralogy and porosity in the barnett shale. J. Geophys. Eng. 10, 25006.

Huang, J.L., Zou, C.N., Li, J.Z., 2012. Shale gas generation and potential of the lower cambrian qiongzhusi formation in the southern Sichuan basin, China. Petrol. Explor. Dev. 39 (1), 75–81.

Hucka, V., Das, B., 1974. Brittleness determination of rocks by different methods. International Journal of Rock Mechanics and Mining Sciences & Geomechanics 11, 389–392.

Huo, Z., Zhang, J., Li, P., Tang, X., Yang, X., 2018. An improved evaluation method for the brittleness index of shale and its application — a case study from the southern north China basin. J. Nat. Gas Sci. Eng. 59, 47–55.

Hurlbut, C.S., Klein, C., 1985. Manual of Mineralogy, 20th ed. John Wiley and Sons, New York, NY, pp. 285–286.

Jarvie, D., Hill, M.R.J., Ruble, T.E., Pollastro, R.M., 2007. Unconventional shale-gas systems: the Mississippian Barnett shale of north-central Texas as one model for thermogenic shale-gas assessment. AAPG Bull. 91, 475–499.

Jiang, L., Zhao, Y., Golsanami, N., Chen, L., Yan, W., 2020. A novel type of neural networks for feature engineering of geological data: case studies of coal and gas hydrate-bearing sediments. Geoscience Frontiers 11 (5), 1511–1531. https://doi.org/10.1016/j.gsf.2020.04.016.

Jin, X.C., Shah, S.N., Roegiers, J.C., Zhang, B., 2014. Fracability evaluation in shale reservoirs-an integrated petrophysics and geomechanics approach. In: SPE Hydraulic Fracturing Technology Conference, The Woodlands, Texas, USA. https://doi.org/10.2118/168589-MS. SPE-168589-MS.

Kang, Y., Shang, C., Zhou, H., et al., 2020. Mineralogical brittleness index as a function of weighting brittle minerals—from laboratory tests to case study. J. Nat. Gas Sci. Eng. 77, 103278. https://doi.org/10.1016/j.jngse.2020.103278.

Kim, T., Seho, H., Jang, S., 2017. Petrophysical approach for S-wave velocity prediction based on brittleness index and total organic carbon of shale gas reservoir: a case study from Horn River Basin, Canada. J. Appl. Geophys. 136, 513–520.

Lashkaripour, G.R., Rastegarnia, A., Ghafoori, M., 2018. Assessment of brittleness and empirical correlations between physical and mechanical parameters of the Asmari limestone in Khersan 2 dam site, in southwest of Iran. J. Afr. Earth Sci. 138, 124–132.

Li, J., Li, W., 2018. A quantitative seismic prediction technique for the brittleness index of shale in the Jiaoshiba Block, Fuling shale gas field in the Sichuan Basin. Nat. Gas. Ind. 5. https://doi.org/10.1016/j.ngib.2017.11.001.

Li, Y., Wang, X., Wu, B., Li, G., Wang, D., 2016. Sedimentary facies of marine shale gas formations in southern China: the lower silurian Longmaxi Formation in the southern Sichuan basin. Journal of Earth Science 27 (5), 807–822.

Li, Z., Li, L., Li, M., Zhang, L., Zhang, Z., Huang, B., Tang, C., 2018. A numerical investigation on the effects of rock brittleness on the hydraulic fractures in the shale reservoir. J. Nat. Gas Sci. Eng. 50, 22–32.

Liang, C., Jiang, Z.X., Yang, Y.T., Wei, X.J., 2012. Shale lithofacies and reservoir space of the Wufeng Longmaxi Formation, Sichuan basin, China. Petrol. Explor. Dev. 39 (6), 736–743.

Liang, C., Jiang, Z.X., Yang, Y.T., Zhang, C., 2016. Deep-water depositional mechanisms and significance for unconventional hydrocarbon exploration: a case study from the lower Silurian Longmaxi shale in the southeastern Sichuan Basin. AAPG (Am. Assoc. Pet. Geol.) Bull. 100 (5), 773–794.

Liu, S., Deng, B., Li, Z., 2012. Architecture of basin-mountain systems and their influences on gas distribution. A case study from the Sichuan basin, south China. J. Asian Earth Sci. 47, 204–215.

Mavko, G., 2008. Petrophysical Manual. University of Science and Technology of China Press, Hefei, pp. 181–199 (in Chinese).

Mcginnis, R.N., Ferrill, D.A., Morris, A.P., Smart, K.J., Lehrmann, D., 2017. Mechanical stratigraphic controls on natural fracture spacing and penetration. J. Struct. Geol. 95, 160–170.

Neter, J., Wasserman, W., Whitmore, G.A., 1988. Applied Statistics, third ed. Allyn and Bacon Inc., London.

Ozfirat, M.K., Hayati, Y., Ferhan, S., Olgay, Y., 2016. A new approach to rock brittleness and its usability at prediction of drillability. J. Afr. Earth Sci. 119, 94–101.

Perez, R., Marfurt, K., 2014. Mineralogy based brittleness prediction from surface seismic data: application to the Barnett Shale. Interpretation 2, T255–T271.

Perez, R., Marfurt, K., 2015. Identification of brittle/ductile areas in unconventional reservoirs using seismic and microseismic data: application to the Barnett

Shale. Interpretation 3, T233–T243.
Qiang, Z., Yasin, Q., Golsanami, N., Du, Q., 2020. Prediction of reservoir quality from log-core and seismic inversion analysis with an artificial neural network: a case study from the sawan gas field, Pakistan. Energies 13 (2), 486. https://doi.org/10.3390/en13020486.
Rickman, R.M., Mullen, E., Petrer, B.G., Kundert, D., 2008. A practical use of shale petrophysics for stimulation design optimization: all shale plays are not clones of the Barnett shale. In: Annual Technical Conference and Exhibition of Society of Petroleum Engineers, Denver, Colorado, USA. SPE-115258-MS.
Ruyue, W., Wenlon, D., Dajian, G., 2015. Logging evaluation method and its application for total organic carbon content in shale: a case study on the Lower Cambrian Niutitang formation in Cengong block, Guizhou Province. J. China Coal Soc. 40 (12), 2874–2883.
Rybacki, E., Reinicke, A., Meier, T., Makasi, M., Dresen, G., 2015. What controls the mechanical properties of shale rocks? – Part I: strength and Young's modulus. J. Petrol. Sci. Eng. 135, 702–722. https://doi.org/10.1016/j.petrol.2015.10.028.
Rybacki, E., Meier, T., Dresen, G., 2016. What controls the mechanical properties of shale rocks? –part II: Brittleness. J. Petrol. Sci. Eng. 144, 39–58. https://doi.org/10.1016/j.petrol.2016.02.022.
Sharma, R.K., Chopra, S., 2013. New attribute for determination of lithology and brittleness. In: AAPG Annual Convention and Exhibition, Long Beach, California, USA. Search and Discovery Article 41155.
Sharma, R.K., Chopra, S., Keay, J., Nemati, H., Lines, L., 2017. Integration of Geomechanical and Mineralogical Data for Fracability Evaluation in Utica Shale Play. SEG International Exposition and 87th Annual Meeting, Houston, TX, USA, pp. 3189–3193.
Shia, X., Liu, G., Cheng, Y., Yang, L., Jiang, H., Chen, L., Jiang, S., Wang, J., 2016. Brittleness index prediction in shale gas reservoirs based on efficient network models. J. Nat. Gas Sci. Eng. 35, 673–685.
Sohail, G.M., Hawkes, C.D., Yasin, Q., 2020. An integrated petrophysical and geomechanical characterization of sembar shale in the lower indus basin, Pakistan, using well logs and seismic data. J. Nat. Gas Sci. Eng. 78, 103327. https://doi.org/10.1016/j.jngse.2020.103327.
Sone, H., Zoback, M., 2013. Mechanical properties of shale gas reservoir rocks – Part 1: static and dynamic elastic properties and anisotropy. Geophysics 78 (5), D381–D392.
Wang, F., 2008. Production fairway: speed rails in gas shale. In: 7th Annual Gas Shales Summit.
Wang, F.P., Gale, J.F.W., 2009. Screening criteria for shale-gas systems. Gulf Coast Association of Geological Societies Transactions 59, 779–793.
Weicht, D., 2015. 3D Seismic Mechanical Stratigraphy and Petrophysical Analysis of the Marcellus Shale in Taylor County. W.V.: thesis. West Virginia University, p. 88.
Wu, Y., Li, X., He, J., Zheng, B., 2016. Mechanical properties of Longmaxi black organic-rich shale samples from south China under uniaxial and triaxial compression states. Energies 9, 1088.
Yang, Y., Hiroki, S., Hows, A., Zoback, M.D., 2013. Comparison of brittleness indices in organic-rich shale formations. In: 47th US Rock Mechanics/Geomechanics Symposium. ARMA, San Francisco, California, USA, pp. 13–403.
Yasin, Q., Du, Q., Sohail, G.M., Ismail, A., 2017. Impact of organic contents and brittleness indices to differentiate the brittle-ductile transitional zone in shale gas reservoir. Geosci. J. 21 (5), 779–789.
Yasin, Q., Du, Q., Sohail, G.M., Ismail, A., 2018a. Fracturing index-based brittleness prediction from geophysical logging data: application to Longmaxi shale. Geomechanics and Geophysics for Geo-Energy and Geo-Resources 4 (4), 301–325.
Yasin, Q., Du, Q., Ismail, A., Yan, D., 2018b. Identification and characterization of natural fractures in gas shale reservoir using conventional and specialized logging tools. In: SEG International Exposition and 88th annual Meeting. SEG Technical Program Expanded Abstracts, Anaheim, CA, pp. 809–813. https://doi.org/10.1190/segam2018-2997626.1.
Yasin, Q., Du, Q., Ismail, A., 2019. A new integrated workflow for improving permeability estimation in a highly heterogeneous reservoir of Sawan Gas Field from well logs data. Geomechanics and Geophysics for Geo-Energy and Geo-Resources 5, 121–142.
Yasin, Q., Yan, D., Ismail, A., Du, Q., 2020. Estimation of petrophysical parameters from seismic inversion by combining particle swarm optimization and multi-layer linear calculator. Nat. Resour. Res. 29, 3291–3317. https://doi.org/10.1007/s11053-020-09641-3.
Yasin, Q., Sohail, G.M., Khalid, P., Baklouti, S., Du, Q., 2021a. Application of machine learning tool to predict the porosity of clastic depositional system, Indus Basin, Pakistan. J. Petrol. Sci. Eng. 197, 107975. https://doi.org/10.1016/j.petrol.2020.107975.
Yasin, Q., Syrine, B., Khalid, P., Du, Q., 2021b. Evaluation of shale-gas reservoirs in complex structural enclosures: a case study from patala shale in kohat-potwar plateau. J. Petrol. Sci. Eng. 198, 108225. https://doi.org/10.1016/j.petrol.2020.108225.
Zhang, C., Dong, D., Wang, Y., Guan, Q., 2017. Brittleness evaluation of the upper ordovician wufeng–lower silurian Longmaxi shale in southern Sichuan basin, China. Energy Explor. Exploit. 35 (4), 430–443.
Zhou, H., Meng, F.Z., Zhang, C.Q., et al., 2014. Quantitative evaluation of rock brittleness based on stress-strain curve. Chin. J. Rock Mech. Eng. 33, 1114–1122.
Zhu, L., Zhang, C., Guo, C., Jiao, Y., Chen, L., Zhou, X., Zhang, C., Zhang, Z., 2018. Calculating the total porosity of shale reservoirs by combining conventional logging and elemental logging to eliminate the effects of gas saturation. Petrophysics 59 (2), 162–184.
Zhu, L., Zhang, C., Zhang, C., Zhang, Z., Zhou, X., Zhu, B., 2019. An improved theoretical nonelectric water saturation method for organic shale reservoirs. IEEE access 7, 51441–51456. Digital Object Identifier 10.1109/ACCESS.2019.2912214.
Zou, C.N., 2011. Unconventional Oil and Gas Geology. Geology Press, Beijing, pp. 76–89 (**In Chinese**).